

UMN-TH-1539/96
 astro-ph/9707212
 May 1997

Primordial Nucleosynthesis and Dark Matter^a

Keith A. Olive

*School of Physics and Astronomy, University of Minnesota,
 Minneapolis, MN 55455, USA*

Following a brief introduction to early Universe cosmology, the current of status of big bang nucleosynthesis is reviewed and the concordance between theory and observation is examined in detail. The abundances of ⁴He and ⁷Li determine the value of the baryon-to-photon ratio, η to be relatively low, $\eta \approx 1.8 \times 10^{-10}$, and agrees with some recent measurements of D/H in quasar absorption systems. These results have far reaching consequences for galactic chemical evolution, the amount of baryonic dark matter in the Universe and on the allowed number of degrees of freedom in the early Universe. Finally, motivations for cosmological dark matter will be reviewed with special emphasis placed on supersymmetric candidates.

1 Introduction

To set the framework for the subsequent discussion on Big Bang Nucleosynthesis (BBN) and dark matter, it will be useful to briefly review some general aspects of the standard hot big bang model. BBN occurs at the relatively late time of order 1 minute after the big bang, however, the initial conditions which determine BBN, were set up much earlier. These include, an isotropic background, a finite baryon density and a period of equilibrium. The standard big bang model assumes homogeneity and isotropy, though it is reasoned that these conditions were achieved after a period of inflation. Given homogeneity and isotropy, space-time can be described by the Friedmann-Robertson-Walker metric which in co-moving coordinates is given by

$$ds^2 = -dt^2 + R^2(t) \left[\frac{dr^2}{(1 - kr^2)} + r^2 (d\theta^2 + \sin^2 \theta d\phi^2) \right] \quad (1)$$

where $R(t)$ is the cosmological scale factor and k is the three-space curvature constant ($k = 0, +1, -1$ for a spatially flat, closed or open Universe). k and R are the only two quantities in the metric which distinguish it from flat Minkowski space. It is also common to assume the perfect fluid form for the energy-momentum tensor described by, the isotropic pressure, p , and the energy density ρ . Einstein's equations yield the Friedmann equation,

$$H^2 \equiv \left(\frac{\dot{R}}{R} \right)^2 = \frac{1}{3} 8\pi G_N \rho - \frac{k}{R^2} + \frac{1}{3} \Lambda \quad (2)$$

^aSummary of lectures given at the 1997 Lake Louise Winter Institute, Lake Louise, Alberta, February 16-20 1997.

and

$$\left(\frac{\ddot{R}}{R}\right) = \frac{1}{3}\Lambda - \frac{1}{6}8\pi G_N(\rho + 3p) \quad (3)$$

where Λ is the cosmological constant, or equivalently from the conservation of the energy momentum tensor

$$\dot{\rho} = -3H(\rho + p) \quad (4)$$

These equations form the basis of the standard big bang model.

At early times ($t < 10^5$ yrs) the Universe is thought to have been dominated by radiation so that the equation of state can be given by $p = \rho/3$. Neglecting the contributions to H from k and Λ (this is always a good approximation for small enough R), we find that

$$R(t) \sim t^{1/2} \quad (5)$$

and $\rho \sim R^{-4}$ so that $t \sim (3/32\pi G_N \rho)^{1/2}$. Similarly for a matter or dust dominated Universe with $p = 0$,

$$R(t) \sim t^{2/3} \quad (6)$$

and $\rho \sim R^{-3}$. The Universe makes the transition between radiation and matter domination when $\rho_{rad} = \rho_{matter}$ or when $T \simeq \text{few} \times 10^3$ K.

In the absence of a cosmological constant, one can define a critical energy density ρ_c such that $\rho = \rho_c$ for $k = 0$

$$\rho_c = 3H^2/8\pi G_N \quad (7)$$

In terms of the present value of the Hubble parameter this is,

$$\rho_c = 1.88 \times 10^{-29} h_o^2 \text{gcm}^{-3} \quad (8)$$

where

$$h_o = H_o/(100\text{kmMpc}^{-1}\text{s}^{-1}) \quad (9)$$

The cosmological density parameter is then defined by

$$\Omega \equiv \frac{\rho}{\rho_c} \quad (10)$$

in terms of which the Friedmann equation, Eq. (2), can be rewritten as

$$(\Omega - 1)H^2 = \frac{k}{R^2} \quad (11)$$

so that $k = 0, +1, -1$ corresponds to $\Omega = 1, \Omega > 1$ and $\Omega < 1$. Broad observational limits on h_o and Ω are¹

$$0.4 \leq h_o \leq 1.0 \quad 0.1 \leq \Omega \leq 2 \quad (12)$$

The value of Ω , at least on relatively small scales, seems to depend on scale. Indeed, the contribution to Ω from visible matter associated with stars and hot gas is quite small, $\Omega \approx 0.003 - 0.01$. On somewhat larger scales, that of galactic halos or small groups of galaxies, $\Omega \approx 0.02 - 0.1$. On galaxy cluster scales, it appears that Ω may be as large as 0.3. And while there is some evidence (see the lectures of N. Kaiser² in these proceedings), the observations are far from conclusive in indicating a value of Ω as large as 1. It is however possible to obtain a bound on the product, Ωh^2 from

$$H_o t_o = \int_0^1 (1 - \Omega + \Omega/x)^{-1/2} dx \quad (13)$$

(for $\Lambda = 0$). For $t_o > 12\text{Gyr}$, and $\Omega \leq 1$, $\Omega h^2 < 0.3$ (This is true even if $\Lambda \neq 0$.)

As indicated above, BBN takes place during the radiation dominated epoch which lasts roughly to the period of recombination (somewhat earlier when dark matter is included) which occurs when electrons and protons form neutral hydrogen through $e^- + p \rightarrow \text{H} + \gamma$ at a temperature $T_R \sim \text{few} \times 10^3 \text{ K} \sim 1 \text{ eV}$. For $T < T_R$, photons are decoupled while for $T > T_R$, photons are in thermal equilibrium. Today, the content of the microwave background consists of photons with $T_o = 2.728 \pm .002 \text{ K}$ ³. The energy density of photons in the background can be calculated from

$$\rho_\gamma = \int E_\gamma dn_\gamma \quad (14)$$

where the density of states is given by

$$dn_\gamma = \frac{g_\gamma}{2\pi^2} [\exp(E_\gamma/T) - 1]^{-1} q^2 dq \quad (15)$$

and $g_\gamma = 2$ is the number of spin polarizations for the photon, $E_\gamma = q$ is just the photon energy (momentum). (I am using units such that $\hbar = c = k_B = 1$ and will do so through the remainder of these lectures.) Integrating (14) gives

$$\rho_\gamma = \frac{\pi^2}{15} T^4 \quad (16)$$

which is the familiar blackbody result.

In general, at very early times, at very high temperatures, other particle degrees of freedom join the radiation background when $T \sim m_i$ for each particle type i if that type is brought into thermal equilibrium through interactions. In equilibrium the energy density of a particle type i is given by

$$\rho_i = \int E_i dn_{q_i} \quad (17)$$

and

$$dn_{q_i} = \frac{g_i}{2\pi^2} [\exp[(E_{q_i} - \mu_i)/T] \pm 1]^{-1} q^2 dq \quad (18)$$

where again g_i counts the total number of degrees of freedom for type i ,

$$E_{q_i} = (m_i^2 + q_i^2)^{1/2} \quad (19)$$

μ_i is the chemical potential if present and \pm corresponds to either Fermi or Bose statistics.

In the limit that $T \gg m_i$ the total energy density can be conveniently expressed by

$$\rho = \left(\sum_B g_B + \frac{7}{8} \sum_F g_F \right) \frac{\pi^2}{30} T^4 \equiv \frac{\pi^2}{30} N(T) T^4 \quad (20)$$

where $g_{B(F)}$ are the total number of boson (fermion) degrees of freedom and the sum runs over all boson (fermion) states with $m \ll T$. The factor of 7/8 is due to the difference between the Fermi and Bose integrals. Equation (20) defines $N(T)$ by taking into account new particle degrees of freedom as the temperature is raised.

In the radiation dominated epoch, eq. (4) can be integrated (neglecting the T -dependence of N) giving us a relationship between the age of the Universe and its temperature

$$t = \left(\frac{90}{32\pi^3 G_N N(T)} \right)^{1/2} T^{-2} \quad (21)$$

Put into a more convenient form

$$t T_{MeV}^2 = 2.4 [N(T)]^{-1/2} \quad (22)$$

where t is measured in seconds and T_{MeV} in units of MeV.

The value of $N(T)$ at any given temperature depends on the particle physics model. In the standard $SU(3) \times SU(2) \times U(1)$ model, we can specify

Table 1: Effective numbers of degrees of freedom in the standard model.

Temperature	New Particles	$4N(T)$
$T < m_e$	γ 's + ν 's	29
$m_e < T < m_\mu$	e^\pm	43
$m_\mu < T < m_\pi$	μ^\pm	57
$m_\pi < T < T_c^*$	π 's	69
$T_c < T < m_{\text{strange}}$	$-\pi$'s + u, \bar{u}, d, \bar{d} + gluons	205
$m_s < T < m_{\text{charm}}$	s, \bar{s}	247
$m_c < T < m_\tau$	c, \bar{c}	289
$m_\tau < T < m_{\text{bottom}}$	τ^\pm	303
$m_b < T < m_{W,Z}$	b, \bar{b}	345
$m_{W,Z} < T < m_{\text{top}}$	W^\pm, Z	381
$m_t < T < m_{\text{Higgs}}$	t, \bar{t}	423
$M_H < T$	H^0	427

* T_c corresponds to the confinement-deconfinement transition between quarks and hadrons. $N(T)$ is shown in Figure 1 for $T_c = 150$ and 400 MeV. It has been assumed that $m_{\text{Higgs}} > m_{\text{top}}$.

$N(T)$ up to temperatures of 0(100) GeV. The change in N can be seen in the following table.

At higher temperatures ($T \gg 100$ GeV), $N(T)$ will be model dependent. For example, in the minimal $SU(5)$ model, one needs to add to $N(T)$, 24 states for the X and Y gauge bosons, another 24 from the adjoint Higgs, and another 6 (in addition to the 4 already counted in W^\pm, Z and H) from the $\bar{5}$ of Higgs. Hence for $T > M_X$ in minimal $SU(5)$, $N(T) = 160.75$. In a supersymmetric model this would at least double, with some changes possibly necessary in the table if the lightest supersymmetric particle has a mass below M_H .

The presence of a particle species in the thermal background assumes thermal equilibrium and hence interaction rates which are sufficiently fast compared with the expansion rate of the Universe. Roughly, this translates to the condition for each particle type i , that some rate Γ_i involving that type be larger than the expansion rate of the Universe or

$$\Gamma_i > H \tag{23}$$

in order to be in thermal equilibrium.

Examples of a processes in equilibrium at early times which drops out of equilibrium or decouples at later times are the processes which involve neutrinos. If we consider the standard neutral or charged-current interactions such

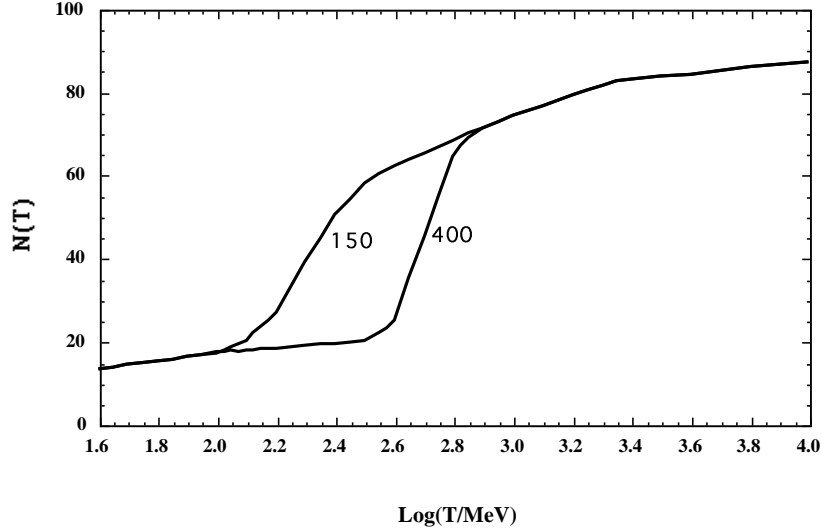


Figure 1: The effective numbers of relativistic degrees of freedom as a function of temperature.

as $e^+ + e^- \leftrightarrow \nu + \bar{\nu}$ or $e + \nu \leftrightarrow e + \nu$ etc., the rates for these processes can be approximated by

$$\Gamma = n \langle \sigma v \rangle \quad (24)$$

where $\langle \sigma v \rangle$ is the thermally averaged weak interaction cross section

$$\langle \sigma v \rangle \sim 0(10^{-2}) T^2 / M_W^4 \quad (25)$$

and n is the number density of leptons. Hence the rate for these interactions is

$$\Gamma_{\text{wk}} \sim 0(10^{-2}) T^5 / M_W^4 \quad (26)$$

The expansion rate, on the other hand, is just

$$H = \left(\frac{8\pi G_N \rho}{3} \right)^{1/2} = \left(\frac{8\pi^3}{90} N(T) \right)^{1/2} T^2 / M_P \sim 1.66 N(T)^{1/2} T^2 / M_P. \quad (27)$$

The Planck mass $M_P = G_N^{-1/2} = 1.22 \times 10^{19}$ GeV.

Neutrinos will be in equilibrium when $\Gamma_{\text{wk}} > H$ or

$$T > (500 M_W^4 / M_P)^{1/3} \sim 1 \text{ MeV}. \quad (28)$$

The temperature at which these rates are equal is commonly referred to as the decoupling or freeze-out temperature and is defined by

$$\Gamma(T_d) = H(T_d) \quad (29)$$

For temperatures $T > T_d$, neutrinos will be in equilibrium, while for $T < T_d$ they will not. Basically, in terms of their interactions, the expansion rate is just too fast and they never “see” the rest of the matter in the Universe (or themselves). Their momenta will simply redshift and their effective temperature (the shape of their momenta distribution is not changed from that of a blackbody) will simply fall with $T \sim 1/R$.

Soon after decoupling the e^\pm pairs in the thermal background begin to annihilate (when $T \lesssim m_e$). Because the neutrinos are decoupled, the energy released heats up the photon background relative to the neutrinos. The change in the photon temperature can be easily computed from entropy conservation. The neutrino entropy must be conserved separately from the entropy of interacting particles. If we denote $T_>$, the temperature of photons, and e^\pm before annihilation, we also have $T_\nu = T_>$ as well. The entropy density of the interacting particles at $T = T_>$ is just

$$s_> = \frac{4\rho_>}{3T_>} = \frac{4}{3}\left(2 + \frac{7}{2}\right)\left(\frac{\pi^2}{30}\right)T_>^3 \quad (30)$$

while at $T = T_<$, the temperature of the photons just after e^\pm annihilation, the entropy density is

$$s_< = \frac{4\rho_<}{3T_<} = \frac{4}{3}(2)\left(\frac{\pi^2}{30}\right)T_<^3 \quad (31)$$

and by conservation of entropy $s_< = s_>$ and

$$(T_</T_>)^3 = 11/4 \quad (32)$$

Thus, the photon background is at higher temperature than the neutrinos because the e^\pm annihilation energy could not be shared among the neutrinos, and

$$T_\nu = (4/11)^{1/3}T_\gamma \simeq 1.9K \quad (33)$$

As we will see below, standard BBN depends on one single parameter, the baryon-to-photon ratio, $\eta = n_B/n_\gamma$. In fact this quantity is really related to the net baryon density $n_B - n_{\bar{B}}$. It would seem however, that today, $n_{\bar{B}} = 0$, and that $n_B/n_\gamma \sim 2 \times 10^{-10}$. In the absence of baryon number violation, this ratio is roughly constant (in an adiabatically expanding Universe, the ratio

of the baryon density to entropy density is constant). The question we face therefore, is what determines these initial conditions, rather than say, $n_B = n_{\bar{B}}$ and/or $n_B/n_\gamma = 1$.

Let us for the moment assume that in fact $\eta = 0$. We can compute the final number density of nucleons left over after annihilations of baryons and antibaryons have frozen out. At very high temperatures, $T > 1$ GeV (but neglecting the quark-hadron transition), nucleons were in thermal equilibrium with the photon background and $n_B = n_{\bar{B}} = (3/2)n_\gamma$ (a factor of 2 accounts for neutrons and protons and the factor 3/4 for the difference between fermi and bose statistics). As the temperature fell below m_N , annihilations kept the nucleon density at its equilibrium value $(n_B/n_\gamma) \simeq (m_N/T)^{3/2}\exp(-m_N/T)$ until the annihilation rate $\Gamma_A \simeq n_B m_\pi^{-2}$ fell below the expansion rate. This occurred at $T \simeq 20$ MeV. However, at this time the nucleon number density had already dropped to

$$n_B/n_\gamma = n_{\bar{B}}/n_\gamma \simeq 10^{-18} \quad (34)$$

which is eight orders of magnitude too small⁴ in addition to the problem of having to separate the baryons from the antibaryons. If any separation did occur at higher temperatures (so that annihilations were as yet incomplete) the maximum distance scale on which separation could occur is the causal scale related to the age of the Universe at that time. At $T = 20$ MeV, the age of the Universe was only $t = 2 \times 10^{-3}$ sec. At that time, a causal region (with distance scale defined by $2ct$) could only have contained $10^{-5}M_\odot$ which is very far from the galactic mass scales on which we are asking for separations to occur, $10^{12}M_\odot$. In spite of all of these problems, $\eta = 0$ implies that the Universe as a whole is baryon symmetric, thus unless baryons are separated on extremely large (inflationary) domains, in which case we might just as well worry again about $\eta \neq 0$, there should be antimatter elsewhere in the Universe. To date, the only antimatter observed is the result of a high energy collision, either in an accelerator or in a cosmic-ray collision in the atmosphere. There has been no sign to date of any primary antimatter, such as an anti-helium nucleus $\bar{\alpha}$ found in cosmic-rays.

The production of a net baryon asymmetry requires baryon number violating interactions, C and CP violation and a departure from thermal equilibrium⁵. The first two of these ingredients are contained in Grand Unified Theories (GUTs), the third can be realized in an expanding universe where as we have seen, it is not uncommon that interactions come in and out of equilibrium. In SU(5), the fact that quarks and leptons are in the same multiplets allows for baryon non-conserving interactions such as $e^- + d \leftrightarrow \bar{u} + \bar{u}$, etc., or decays of the supermassive gauge bosons X and Y such as $X \rightarrow e^- + d, \bar{u} + \bar{u}$. Although

today these interactions are very ineffective because of the very large masses of the X and Y bosons, in the early Universe when $T \sim M_X \sim 10^{15}$ GeV these types of interactions should have been very important. C and CP violation is very model dependent. In the minimal SU(5) model the magnitude of C and CP violation is too small to yield a useful value of η . The C and CP violation in general comes from the interference between tree level decay diagrams and their one loop corrections.

The departure from equilibrium is very common in the early Universe when interaction rates cannot keep up with the expansion rate. In fact, the simplest (and most useful) scenario for baryon production makes use of the fact that a single decay rate goes out of equilibrium. It is commonly referred to as the out of equilibrium decay scenario⁶. The basic idea is that the gauge bosons X and Y (or Higgs bosons) may have a lifetime long enough to insure that the inverse decays have already ceased so that the baryon number is produced by their free decays.

More specifically, let us call X either the gauge boson or Higgs boson, which produces the baryon asymmetry through decays. Let α be its coupling to fermions. For X a gauge boson, α will be the GUT fine structure constant, while for X a Higgs boson, $(4\pi\alpha)^{1/2}$ is its Yukawa coupling to fermions. The decay rate for X will be

$$\Gamma_D \simeq \alpha M_X \quad (35)$$

However decays can only begin occurring when the age of the Universe is longer than the X lifetime Γ_D^{-1} , i.e., when $\Gamma_D > H$

$$\alpha M_X \gtrsim N(T)^{1/2} T^2 / M_P \quad (36)$$

or at a temperature

$$T^2 \lesssim \alpha M_X M_P N(T)^{-1/2}. \quad (37)$$

Scatterings on the other hand proceed at a rate $\Gamma_S \sim \alpha^2 T^3 / M_X^2$ and hence are not effective at lower temperatures. To be in equilibrium, decays must have been effective as T fell below M_X in order to track the equilibrium density of X 's (and \bar{X} 's). Therefore, the out-of-equilibrium condition is that at $T = M_X$, $\Gamma_D < H$ or

$$M_X \gtrsim \alpha M_P (N(M_X))^{-1/2} \sim 10^{18} \alpha \text{GeV} \quad (38)$$

In this case, we would expect a maximal net baryon asymmetry to be produced.

In the out-of-equilibrium decay scenario⁶, the total baryon asymmetry produced per X, \bar{X} pair is proportional to $\Delta B = (\bar{r} - r)$ as can easily be seen from Figure 2. Here r (\bar{r}) is the relevant branching ratio for the decay of X

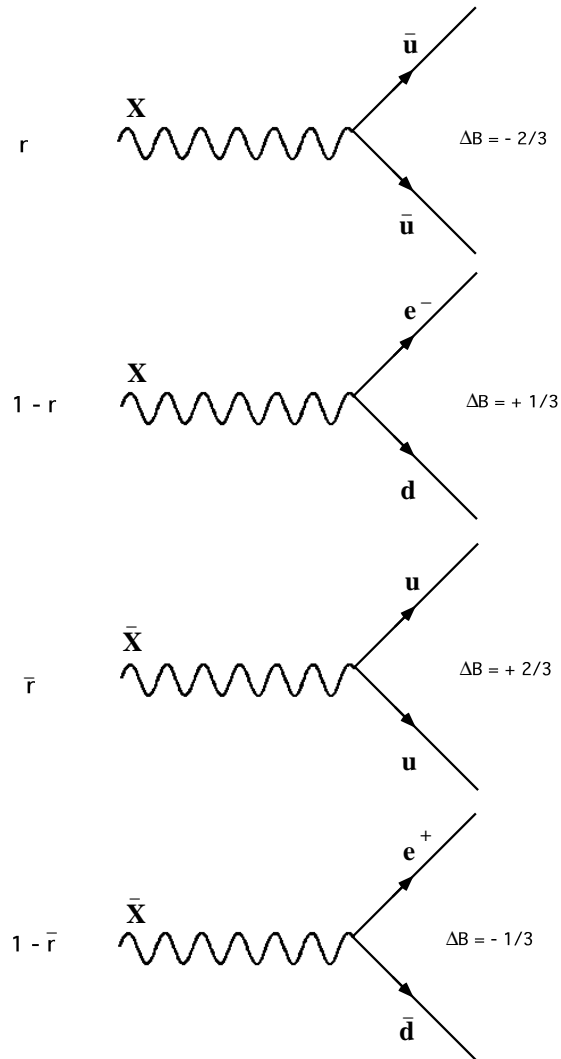


Figure 2: The baryon number violating decays of X and \bar{X} .

(\bar{X}). C and CP violation translate into the condition that $r \neq \bar{r}$. If decays occur out-of-equilibrium, then at the time of decay, $n_X \approx n_\gamma$ at $T < M_X$. We then have

$$\frac{n_B}{s} = \frac{(\Delta B)n_X}{s} \sim \frac{(\Delta B)n_X}{N(T)n_\gamma} \sim 10^{-2}(\Delta B) \quad (39)$$

Some comments regarding the baryogenesis mechanism described above are in order: Initial conditions are not important. Equilibrium prior to decay erases any net baryon number. The out of equilibrium decays of X and Y then generate a new asymmetry. Therefore, the final resulting asymmetry is always the same, given by say, (39). While $n_B/s \sim 10^{-10}$ is possible, the final result is strongly model dependent. I should add that several other mechanisms for baryogenesis are known to exist⁷, but all require the same three key ingredients.

There are several long standing cosmological problems whose solution we associate with inflation (see refs. 2 and 8). Here I will describe only one of these. The curvature problem (or flatness problem or age problem) can manifest itself in several ways. For a radiation dominated gas, the entropy density $s \sim T^3$ and conservation of entropy implies $R \sim T^{-1}$. Thus assuming an adiabatically expanding Universe, the quantity $\hat{k} = k/R^2T^2$ is a dimensionless constant. If we now apply the limit in Eq. (12) to Eq. (11) we find

$$\hat{k} = \frac{k}{R^2T^2} = \frac{(\Omega_o - 1)H_o^2}{T_o^2} < 2 \times 10^{-58} \quad (40)$$

This limit on k represents an initial condition on the cosmological model. The problem is: what physical processes in the early Universe produced a value of \hat{k} so extraordinarily close to zero (or Ω close to one)? A more natural initial condition might have been $\hat{k} \sim 0(1)$. In this case the Universe would have become curvature dominated at $T \sim 10^{-1}M_P$.

It is important to note that Ω is a function of time or of the scale factor. The evolution of Ω is shown in Figure 3 for $\Lambda = 0$. For a spatially flat Universe, $\Omega = 1$ always. When $k = +1$, there is a maximum value for the scale factor R . At early times (small values of R), Ω always tends to one. Note that the fact that we do not yet know the sign of k , or equivalently whether Ω is larger than or smaller than unity, implies that we are at present still at the very left in the figure. What makes this peculiar is that one would normally expect that the sign of k to become apparent after a Planck time of 10^{-43} s. It is extremely puzzling that some 10^{60} Planck times later, we still do not know the sign of k .

The curvature problem discussed above among others can be neatly resolved if the Universe underwent a period of cosmological inflation⁸. During a phase transition, our assumptions of an adiabatically expanding universe may

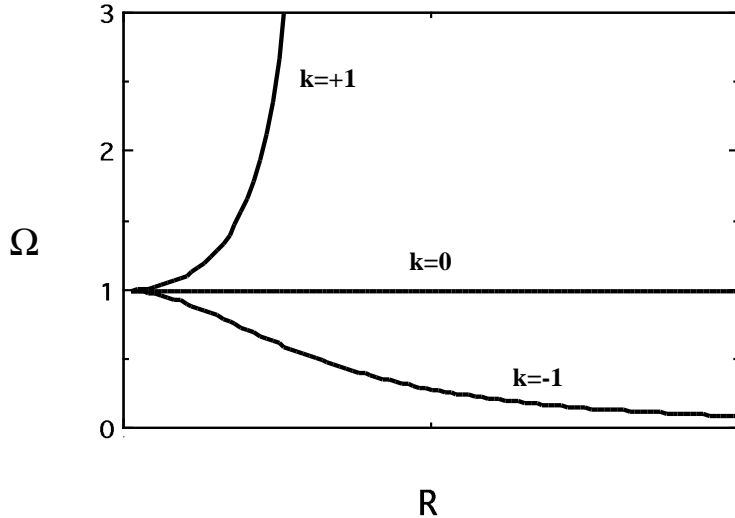


Figure 3: The evolution of the cosmological density parameter, Ω , as a function of the scale factor for a closed, open and spatially flat Universe.

not be valid. If we look at a scalar potential describing a phase transition from a symmetric false vacuum state $\langle\phi\rangle = 0$ for some scalar field ϕ to the broken true vacuum at $\langle\phi\rangle = v$, and suppose we find that upon solving the equations of motion for the scalar field that the field evolves slowly from the symmetric state to the global minimum (this will depend on the details of the potential). If the evolution is slow enough, the universe may become dominated by the vacuum energy density associated with the potential near $\phi \approx 0$. The energy density of the symmetric vacuum, $V(0)$ acts as a cosmological constant with

$$\Lambda = 8\pi V(0)M_P^2 \quad (41)$$

During this period of slow evolution, the energy density due, to say, radiation will fall below the vacuum energy density, $\rho \ll V(0)$. When this happens, the expansion rate will be dominated by the constant $V(0)$ and from Eq. (2) we find an exponentially expanding solution

$$R(t) \sim e^{\sqrt{\Lambda/3} t} \quad (42)$$

When the field evolves towards the global minimum it will begin to oscillate about the minimum, energy will be released during its decay and a hot thermal

universe will be restored. If released fast enough, it will produce radiation at a temperature $T_R^4 \lesssim V(0)$. In this reheating process entropy has been created and $(RT)_f > (RT)_i$. Thus we see that during a phase transition the relation $RT \sim \text{constant}$, need not hold true and thus our dimensionless constant \hat{k} may actually not have been constant.

If during the phase transition, the value of RT changed by a factor of $0(10^{29})$, the cosmological problems would be solved. The isotropy would in a sense be generated by the immense expansion; one small causal region could get blown up and hence our entire visible Universe would have been at one time in thermal contact. In addition, the parameter \hat{k} could have started out $0(1)$ and have been driven small by the expansion.

2 Big Bang Nucleosynthesis

The concordance between big bang nucleosynthesis (BBN) theory and observation has been the subject of considerable recent debate. It is clear however, that the real questions lie not with the concordance between BBN and the observational data, but rather between the theories of chemical and stellar evolution and the data. BBN theory (see for example ref. 9) is quite stable in the sense that over time very little in the fundamental theory has changed. Cross-sections are now more accurately measured, the neutron mean life is known with a much higher degree of precision, and if we restrict our attention to the standard model, the number of neutrinos has also been determined. In contrast, the status of the observational data has changed significantly in the last several years. There is better data on ^4He , more data on ^7Li , and data on D and ^3He that was simply non-existent several years ago. For the most part, the inferred abundances of ^4He and ^7Li have remained relatively fixed, giving us a higher degree of confidence in the assumed primordial abundances of these isotopes as is reflected in their observational uncertainties. Indeed, the abundances of ^4He and ^7Li alone are sufficient in order to probe and test the theory and determine the single remaining parameter in the standard model¹⁰, namely, the baryon-to-photon ratio, η . In contrast, D and ^3He are highly dependent on models of chemical evolution (^3He is in addition dependent on the uncertain stellar yields of this isotope). New data from quasar absorption systems, on what may be primordial D/H is at this time discordant, different measurements give different abundances. As a consequence of the uncertainties in D and ^3He , one can use the predictions based on ^4He and ^7Li in order to construct models of galactic chemical evolution. These results also have important implications for the amount of (non)-baryonic dark matter in the galaxy and on the number of allowed relativistic degrees of freedom at the

time of BBN, commonly parameterized as N_ν . The basic results of BBN are summarized in Figure 4, showing the range in η where consistency with the observations is achieved.

There has always been an intimate connection between BBN and the microwave background as key test to the standard big bang model. Indeed, it was the formulation of BBN which predicted the existence of the microwave background radiation¹¹. The argument is rather simple. BBN requires temperatures greater than 100 keV, which according to eqs. (21) and (22) corresponds to timescales less than about 200 s. The typical cross section for the first link in the nucleosynthetic chain is

$$\sigma v(p + n \rightarrow D + \gamma) \simeq 5 \times 10^{-30} \text{cm}^3/\text{s} \quad (43)$$

This implies that it was necessary to achieve a density

$$n \sim \frac{1}{\sigma v t} \sim 10^{17} \text{cm}^{-3} \quad (44)$$

Now the density in baryons today is known approximately from the density of visible matter to be $n_{B_o} \sim 10^{-7} \text{cm}^{-3}$ and since we know that that the density n scales as $R^{-3} \sim T^3$, the temperature today must be

$$T_o = (n_{B_o}/n)^{1/3} T_{\text{BBN}} \sim 10\text{K} \quad (45)$$

A pretty good estimate.

Despite its simplicity, BBN was criticized early on, due to its shortcomings in being able to produce the observed abundances of *all* of the element isotopes. Attention was therefore turned to stellar nucleosynthesis. However, while the elements from helium on up can be and are produced in stars, no other astrophysical site has ever survived for the production of deuterium. In addition, if one assumes that ${}^4\text{He}$ is entirely of stellar origin, one should be able to find places in the Universe in which the ${}^4\text{He}$ mass fraction is substantially below 25%. The ${}^4\text{He}$ data shown in Figure 5, emphasizes the fact that indeed no such region with low ${}^4\text{He}$ has ever been observed and that (together with the need to produce D) leads one to conclude that BBN nucleosynthesis is a necessary component in any cosmological model.

Before commencing with the direct comparison between theory and observations, it will be useful to briefly review the main events leading to the synthesis of the light elements. Conditions for the synthesis of the light elements were attained in the early Universe at temperatures $T \lesssim 1 \text{MeV}$. At somewhat higher temperatures, weak interaction rates were in equilibrium, thus fixing the ratio of number densities of neutrons to protons. At $T \gg 1$

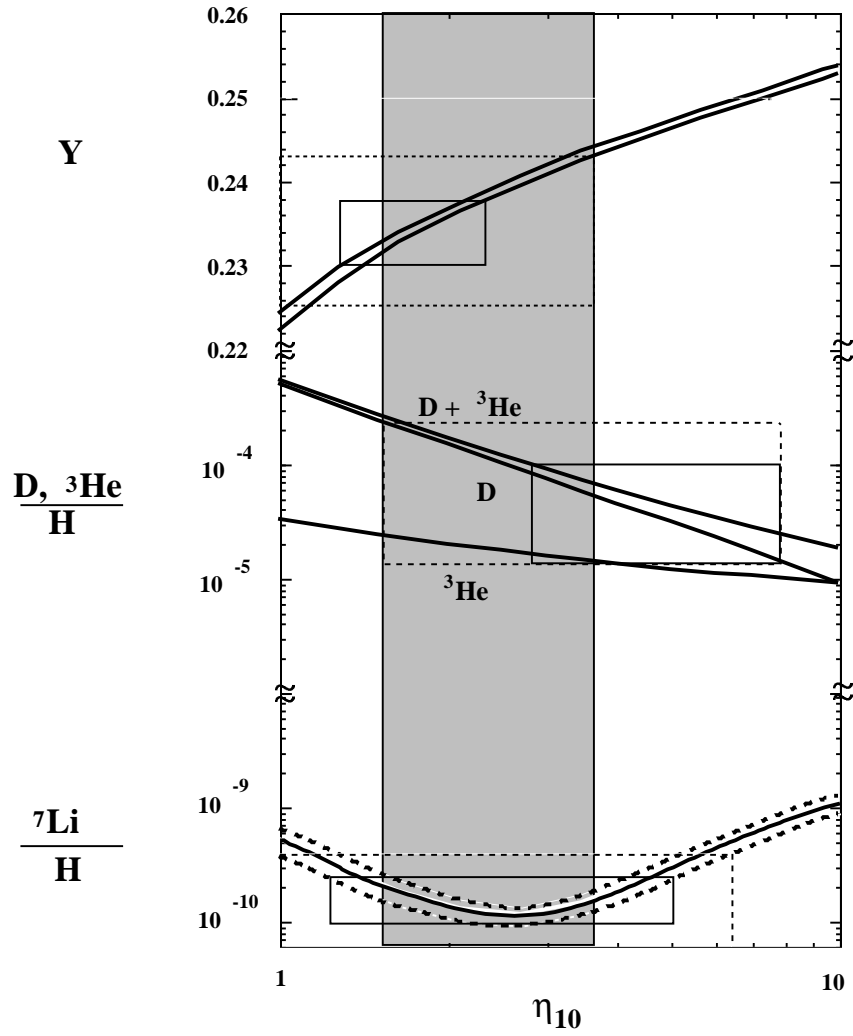


Figure 4: The light element abundances from big bang nucleosynthesis as a function of $\eta_{10} = 10^{10}\eta$.

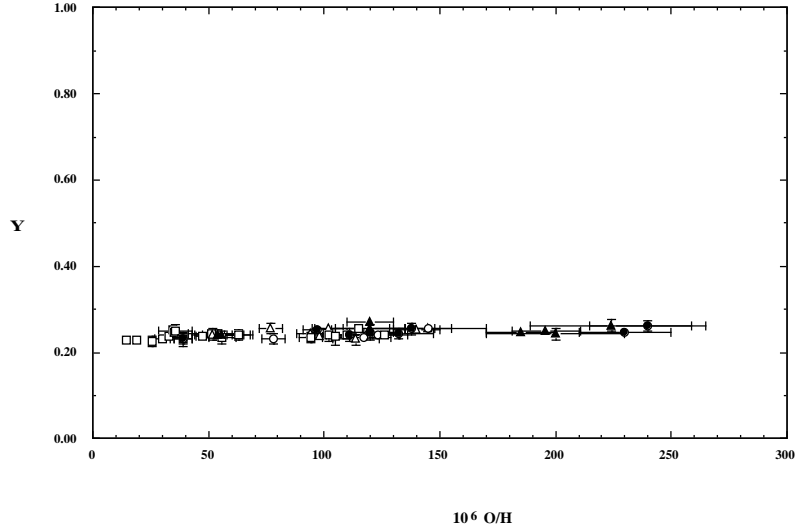


Figure 5: The helium (Y) vs oxygen (O/H) abundances in extragalactic HII regions emphasizing the lack of low ${}^4\text{He}$ regions.

MeV, $(n/p) \simeq 1$. As the temperature fell and approached the point where the weak interaction rates were no longer fast enough to maintain equilibrium, the neutron to proton ratio was given approximately by the Boltzmann factor, $(n/p) \simeq e^{-\Delta m/T}$, where Δm is the neutron-proton mass difference. The final abundance of ${}^4\text{He}$ is very sensitive to the (n/p) ratio.

The nucleosynthesis chain begins with the formation of deuterium through the process, $p+n \rightarrow \text{D} + \gamma$. However, because the large number of photons relative to nucleons, $\eta^{-1} = n_\gamma/n_B \sim 10^{10}$, deuterium production is delayed past the point where the temperature has fallen below the deuterium binding energy, $E_B = 2.2$ MeV (the average photon energy in a blackbody is $\bar{E}_\gamma \simeq 2.7T$). When the quantity $\eta^{-1}\exp(-E_B/T) \sim 1$ the rate for deuterium destruction ($\text{D} + \gamma \rightarrow p + n$) finally falls below the deuterium production rate and the nuclear chain begins at a temperature $T \sim 0.1\text{MeV}$. The nuclear chain in BBN calculations was extended¹² and is shown in Figure 6.

The dominant product of big bang nucleosynthesis is ${}^4\text{He}$ resulting in an abundance of close to 25% by mass. This quantity is easily estimated by counting the number of neutrons present when nucleosynthesis begins. When the weak interaction rates responsible for $n - p$ equilibrium freeze-out, at $T \approx 0.8$ MeV, the neutron to proton ratio is about 1/6. When free neutron decays

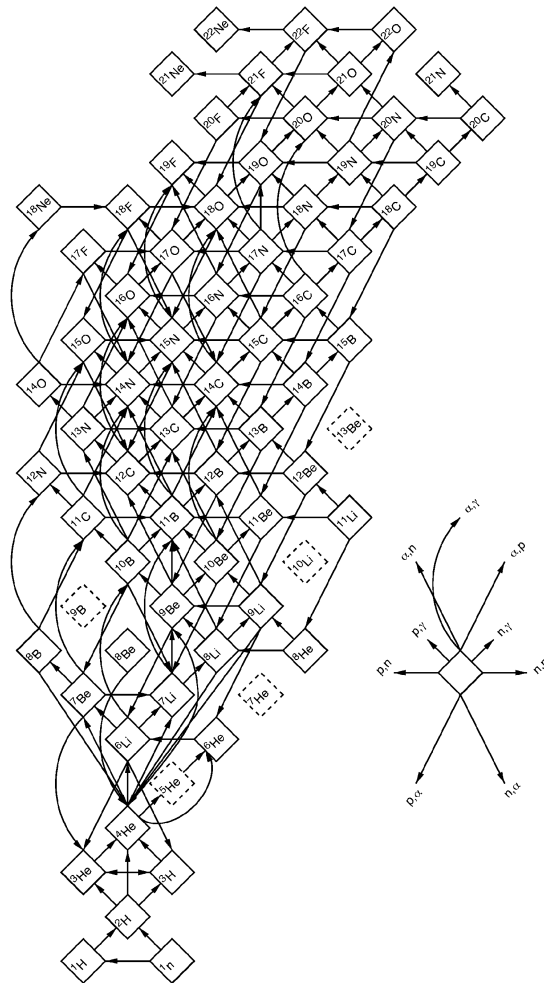


Figure 6: The nuclear network used in BBN calculations.

prior to deuterium formation are taken into account, the ratio drops to $(n/p) \approx 1/7$. Then simple counting yields a ${}^4\text{He}$ mass fraction

$$Y_p = \frac{2(n/p)}{[1 + (n/p)]} \approx 0.25 \quad (46)$$

In the standard model, the ${}^4\text{He}$ mass fraction depends primarily on the baryon to photon ratio, η as it is this quantity which determines the onset of nucleosynthesis via deuterium production. For larger values of η , the quantity $\eta^{-1}\exp(-E_B/T) \sim 1$ is smaller, and hence the nuclear chain may begin at a higher temperature. As a result, the (n/p) ratio is higher, producing more ${}^4\text{He}$. But because the (n/p) ratio is only weakly dependent on η , the ${}^4\text{He}$ mass fraction is relatively flat as a function of η . When we go beyond the standard model, the ${}^4\text{He}$ abundance is very sensitive to changes in the expansion rate which can be related to the effective number of neutrino flavors as will be discussed below. Lesser amounts of the other light elements are produced: D and ${}^3\text{He}$ at the level of about 10^{-5} by number, and ${}^7\text{Li}$ at the level of 10^{-10} by number. These abundances (along with ${}^6\text{Li}$) are shown in Figure 7¹². In Figure 8, the produced abundances of the intermediate mass isotopes ${}^9\text{Be}$, ${}^{10}\text{B}$, ${}^{11}\text{B}$ are also shown. These abundances are far below the observed values and it is believed that these isotopes are formed in cosmic ray nucleosynthesis.

For the comparison with the observations, I will use the resulting abundances of the light elements shown in Figure 4. The curves for the ${}^4\text{He}$ mass fraction, Y , bracket the computed range based on the uncertainty of the neutron mean-life which has been taken as¹³ $\tau_n = 887 \pm 2$ s. Uncertainties in the produced ${}^7\text{Li}$ abundances have been adopted from the results in Hata et al.¹⁴. Uncertainties in D and ${}^3\text{He}$ production are small on the scale of this figure. The boxes correspond to the observed abundances and will be discussed below.

2.1 Light Element Abundances

There is now a good collection of abundance information on the ${}^4\text{He}$ mass fraction, Y , O/H, and N/H in over 70 extragalactic HII (ionized hydrogen) regions^{15,16,17}. The ${}^4\text{He}$ abundance in very low metallicity regions is best determined from observations of $\text{HeII} \rightarrow \text{HeI}$ recombination lines. The observation of the heavy elements is important as the helium mass fraction observed in these HII regions has been augmented by some stellar processing, the degree to which is given by the oxygen and nitrogen abundances. In an extensive study based on the data in^{15,16}, it was found¹⁸ that the data is well represented by a linear correlation for Y vs. O/H and Y vs. N/H. It is then expected that the primordial abundance of ${}^4\text{He}$ can be determined from the intercept of that

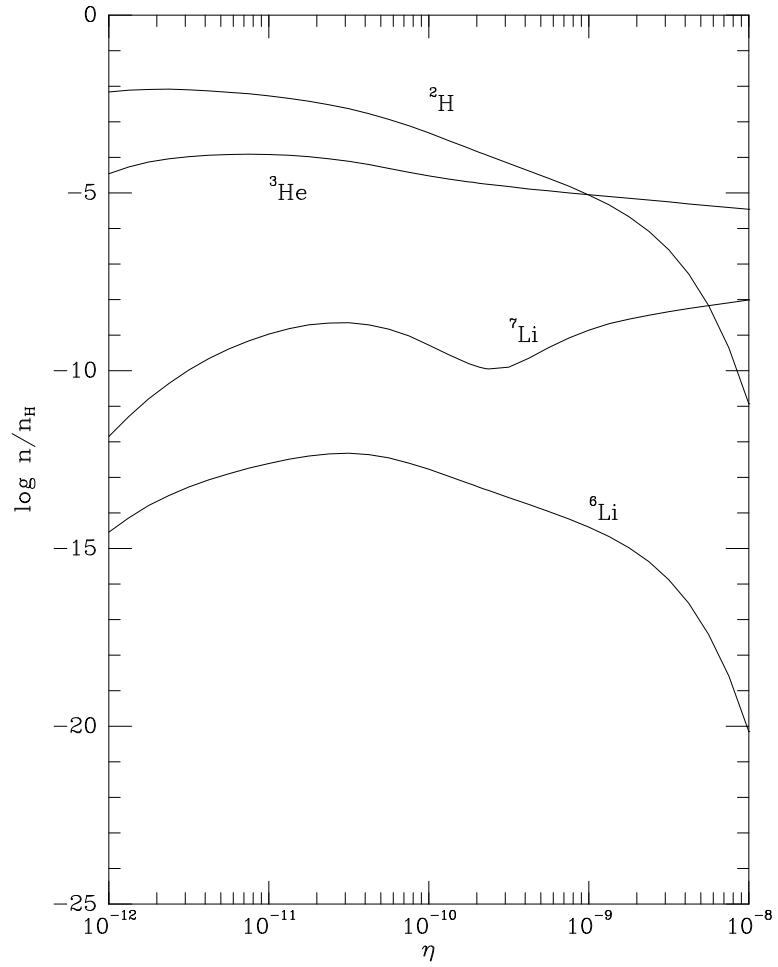


Figure 7: The light element abundances from big bang nucleosynthesis as a function of η , including ^6Li .

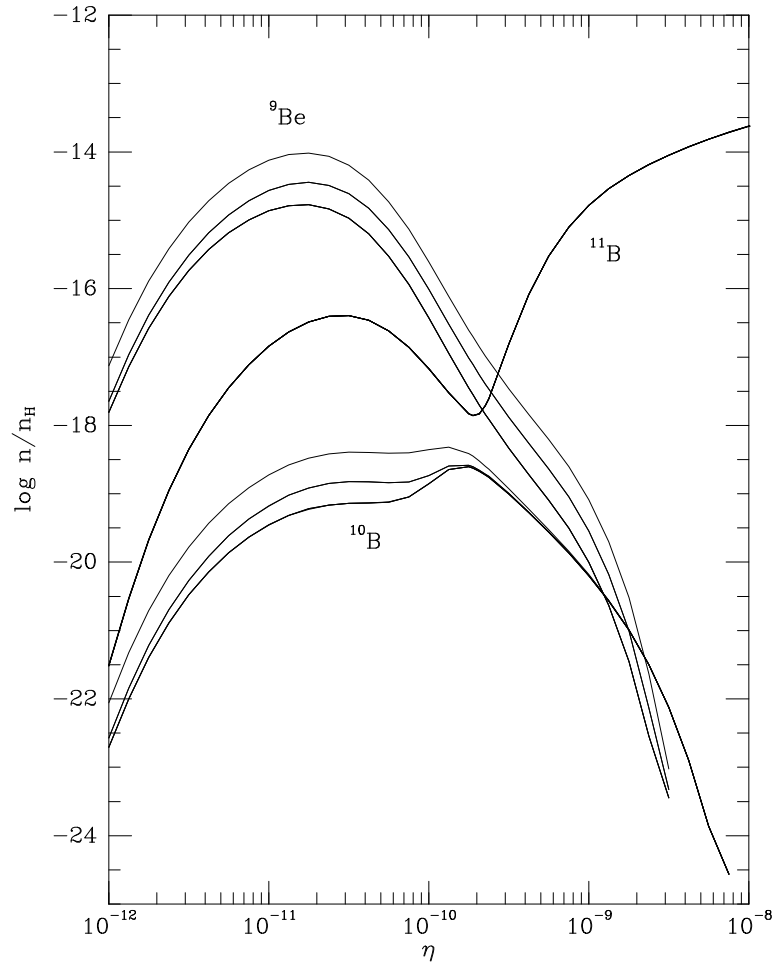


Figure 8: The intermediate mass element abundances from big bang nucleosynthesis as a function of η .

relation. The overall result of that analysis indicated a primordial mass fraction, $Y_p = 0.232 \pm 0.003$. The stability of this fit was verified by a statistical bootstrap analysis¹⁹ showing that the fits were not overly sensitive to any particular HII region.

To make use of the ^4He data, it is crucial to obtain high quality and very low metallicity data. In principle, any one HII region (with non-zero metallicity) should provide an upper limit to Y_p since some stellar processing has taken place augmenting the primordial value. Thus the determination of Y_p by an extrapolation to zero metallicity could be avoided by the observations of either low metallicity or low helium HII regions. For a very low metallicity HII region such an upper limit may even provide a reasonable estimate of Y_p . For example, I Zw 18, is the lowest metallicity extragalactic HII region with ^4He observed. In I Zw 18, there are 2 separate regions, and there have been five distinct measurements of ^4He . In the HII regions designated as NW and SE, the five measured abundances are shown in the table below. This data

TABLE 1: DATA FOR I ZW 18

NW	$.216 \pm .012$	ref. 15
NW	$.231 \pm .006$	ref. 16
NW	$.232 \pm .008$	ref. 17
SE	$.231 \pm .012$	ref. 15
SE	$.230 \pm .008$	ref. 16

leads to a total average for I Zw 18 of $Y_p = 0.230 \pm 0.004$. There are several other regions with low ^4He abundances and the value of Y derived from the average of several HII regions is also of interest²⁰. If we successively include additional HII regions with higher Y , as more regions are included, the mean value (weighted) of Y will increase, but if the errors are statistical, the error in the mean will decrease. As a result, for N HII regions the one-(or two-) σ upper bound to Y will first decrease with N , then level off and, as N is further increased, it will eventually increase monotonically. This behavior is seen in Figure 9 where weighted means are shown, and the 1σ bounds to the weighted means of Y derived from the N lowest helium abundance HII regions. Note that for $2 \leq N \leq 13$, the mean varies from 0.229 to 0.231 while for $2 \leq N \leq 14$, $\langle Y \rangle \leq 0.236(2\sigma)$. It is not unreasonable to infer from these results that,

$$Y_p \leq 0.230 \pm 0.003 \quad (47)$$

with, $Y_p^{2\sigma} \leq 0.236$. If, instead, we take the weighted means of the regions with the lowest values of O/H, we obtain a similar result. This illustrates

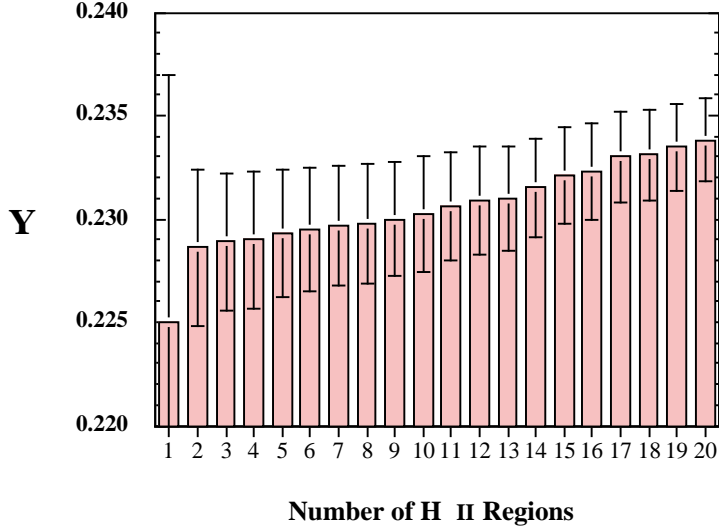


Figure 9: The running average (weighted means) of the ${}^4\text{He}$ abundance, Y , for the first N (lowest Y) HII regions (from ref. 20). Also shown are the 1σ bounds to the weighted means.

the potentially great value of very careful analyses of a handful of the lowest metallicity (lowest Y) HII regions.

Although the above estimates on Y_p are consistent with those based on a linear extrapolation of the data in refs. 15 and 16, it has been claimed, that the new data in ref. 17, leads to a significantly higher value for Y_p (in excess of 24%). However, in a recent analysis²⁰ it has been shown that the data in ref. 17 is entirely consistent with the data in refs. 15 and 16 as can be seen in Figure 10 where the Y versus O/H data used in ref. 18 (open circles, based on the data in refs. 15 and 16)) is shown along with the new data (filled circles, from ref. 17). The crossed circles are the 10 HII regions that Izotov et al. excluded from their own analyses. Note that where there is overlap in O/H , the newer Y values are intermingled with those from refs 15 and 16. It was argued²⁰ that because the data in ref. 17 does not extend down to sufficiently low metallicity, taken alone it can not be used to determine Y_p . It was also shown²⁰ that one can not argue for a systematic shift in Y on the basis of new atomic data calculations as was done in ref. 17. On the other hand, this data may be combined with the previous data in which case one finds a ${}^4\text{He}$ mass fraction²⁰ based on 62 distinct HII regions

$$Y_p = 0.234 \pm 0.002 \pm 0.005 \quad (48)$$

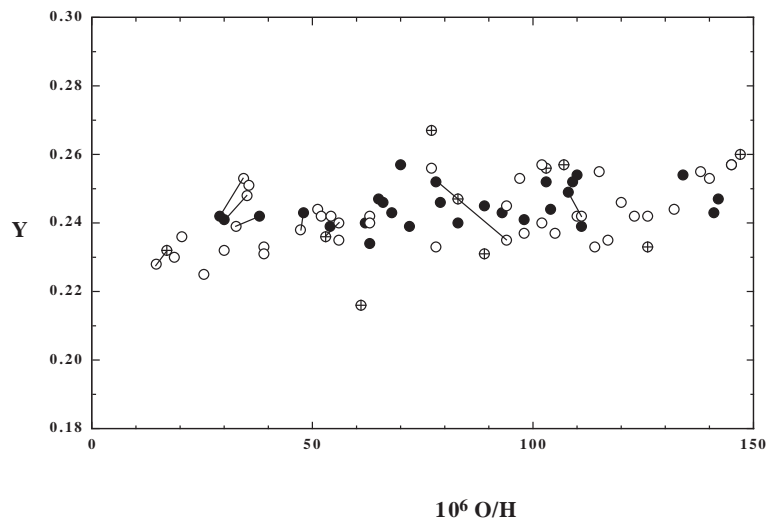


Figure 10: The helium (Y) and oxygen (O/H) abundances from ref. 20 in extragalactic HII regions, (open circles) from refs. 15 and 16, and from ref. 17 (filled circles). Regions excluded by ref. 17 are shown as crossed circles. Lines connect the same regions observed by different groups.

The first uncertainty is purely statistical and the second uncertainty is an estimate of the systematic uncertainty in the primordial abundance determination. The solid box for ${}^4\text{He}$ in Figure 4 represents the range (at $2\sigma_{\text{stat}}$) from (48). The dashed box extends this by σ_{sys} . A somewhat lower primordial abundance of $Y_p = 0.230 \pm .003$ is found by restricting to the 32 most metal poor regions

The ${}^7\text{Li}$ abundance is also reasonably well known. In old, hot, population-II stars, ${}^7\text{Li}$ is found to have a very nearly uniform abundance. For stars with a surface temperature $T > 5500$ K and a metallicity less than about 1/20th solar (so that effects such as stellar convection may not be important), the abundances show little or no dispersion beyond that which is consistent with the errors of individual measurements. Indeed, as detailed in ref. 21, much of the work concerning ${}^7\text{Li}$ has to do with the presence or absence of dispersion and whether or not there is in fact some tiny slope to a $[\text{Li}] = \log {}^7\text{Li}/\text{H} + 12$ vs. T or $[\text{Li}]$ vs. $[\text{Fe}/\text{H}]$ relationship ($[\text{Fe}/\text{H}]$ is the log of the Fe/H ratio relative to the solar value).

There is ${}^7\text{Li}$ data from nearly 100 halo stars, from a variety of sources. When the Li data from stars with $[\text{Fe}/\text{H}] < -1.3$ is plotted as a function of surface temperature, one sees a plateau emerging for $T > 5500$ K as shown in Figure 11 for the data taken from ref. 22. As one can see from the figure, at high temperatures, where the convection zone does not go deep below the surface, the Li abundance is uniform. At lower temperatures, the surface abundance of Li is depleted as Li passes through the interior of the star and is destroyed. The lack of dispersion in the plateau region is evidence that this abundance is indeed primordial (or at least very close to it). Another way to see the plateau is to plot the Li abundance data as a function of metallicity, this time with the restriction that $T > 5500$ K as seen in Figure 12. In this case, the plateau emerges at low $[\text{Fe}/\text{H}]$ as would be expected. At higher $[\text{Fe}/\text{H}]$, the convection zone remains below the surface only for much hotter stars. Thus, for $[\text{Fe}/\text{H}] > -1.3$, the effects of depletion are seen. Also apparent in this figure is that at higher metallicities there is evidence for the production of Li which rises by over an order of magnitude at solar metallicity.

I will use the value given in ref. 22 as the best estimate for the mean ${}^7\text{Li}$ abundance and its statistical uncertainty in halo stars

$$\text{Li}/\text{H} = (1.6 \pm 0.1_{-0.3}^{+0.4+1.6}) \times 10^{-10} \quad (49)$$

The first error is statistical, and the second is a systematic uncertainty that covers the range of abundances derived by various methods. The Li abundance is somewhat sensitive to stellar parameters such as the assumed surface temperature, the metallicity and the surface gravity. The greatest model de-

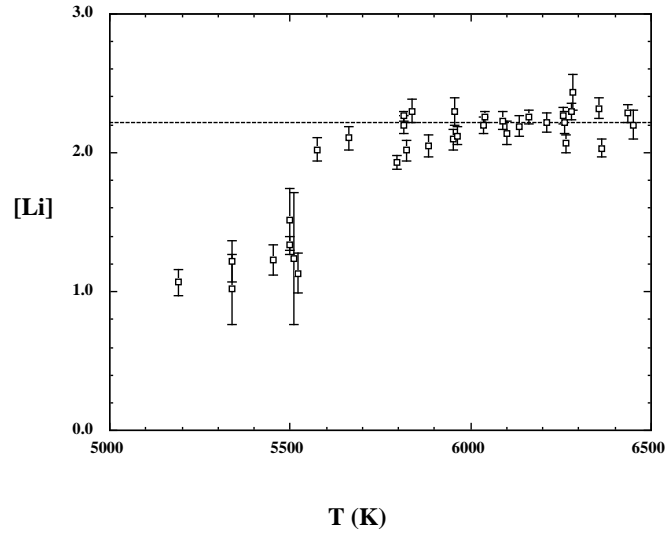


Figure 11: The Li abundance in halo stars with $[\text{Fe}/\text{H}] < -1.3$, as a function of surface temperature

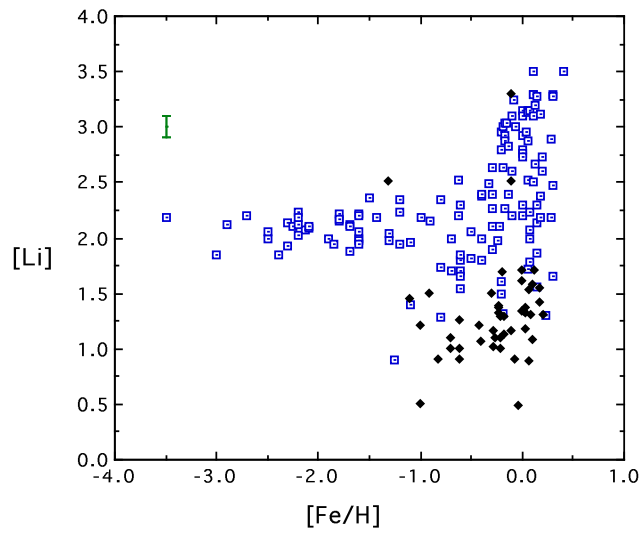


Figure 12: The Li abundance in halo stars with $T > 5500$ K, as a function of metallicity. Filled diamonds represent upper limits.

pendence is on the conversion of the observed colors (B-V) to temperature. For example, in a sample of 55 stars taken from the papers of ref. 23, one finds $[\text{Li}] = 2.08 \pm 0.02$. From Thorburn's²⁴ sample of 74 stars one finds $[\text{Li}] = 2.26 \pm 0.01$. And ref. 22, which comprises 41 stars gives $[\text{Li}] = 2.21 \pm 0.01$. The Li abundance used in (49) is derived from this last data set. The solid box for ${}^7\text{Li}$ in Figure 4 represents the $2\sigma_{\text{stat}} + \sigma_{\text{sys}}$ range from (49).

The third set of errors deals with the possible depletion and/or production of ${}^7\text{Li}$. These uncertainties are however limited. As was noted above, the lack of dispersion in the Li data limits the amount of depletion. In addition, standard stellar models²⁵ predict that any depletion of ${}^7\text{Li}$ would be accompanied by a very severe depletion of ${}^6\text{Li}$. Until recently, ${}^6\text{Li}$ had never been observed in hot pop II stars. The observation²⁶ of ${}^6\text{Li}$ (which turns out to be consistent with its origin in cosmic-ray nucleosynthesis and with a small amount of depletion as expected from standard stellar models) is another good indication that ${}^7\text{Li}$ has not been destroyed in these stars²⁷.

Aside from the big bang, Li is produced together with Be and B in cosmic ray spallation of C,N,O by protons and α -particles. Li is also produced by $\alpha - \alpha$ fusion. Be and B have been observed in these same pop II stars and in particular there are a dozen or so stars in which both Be and ${}^7\text{Li}$ have been observed. Thus Be (and B though there is still a paucity of data) can be used as a consistency check on primordial Li²⁸. Based on the Be abundance found in these stars, one can conclude that no more than 10-20% of the ${}^7\text{Li}$ is due to cosmic ray nucleosynthesis leaving the remainder (an abundance near 10^{-10}) as primordial. The third set of errors in Eq. (49) accounts for the possibility that as much as half of the primordial ${}^7\text{Li}$ has been destroyed in stars, and that as much as 20% of the observed ${}^7\text{Li}$ may have been produced in cosmic ray collisions rather than in the Big Bang. The dashed box in Figure 4, accounts for this additional uncertainty. For ${}^7\text{Li}$, the uncertainties are clearly dominated by systematic effects.

Turning to D/H, we have three basic types of abundance information: 1) ISM data, 2) solar system information, and perhaps 3) a primordial abundance from quasar absorption systems. The best measurement for ISM D/H is²⁹

$$(\text{D}/\text{H})_{\text{ISM}} = 1.60 \pm 0.09_{-0.10}^{+0.05} \times 10^{-5} \quad (50)$$

Because there are no known astrophysical sites for the production of deuterium, all observed D must be primordial. As a result, a firm lower bound from deuterium establishes an upper bound on η which is robust and is shown by the lower right of the solid box in Figure 4. The solar abundance of D/H is inferred from two distinct measurements of ${}^3\text{He}$. The solar wind measurements of ${}^3\text{He}$ as well as the low temperature components of step-wise heating measurements

of ${}^3\text{He}$ in meteorites yield the presolar $(\text{D} + {}^3\text{He})/\text{H}$ ratio, as D was efficiently burned to ${}^3\text{He}$ in the Sun's pre-main-sequence phase. These measurements indicate that^{30,31}

$$\left(\frac{\text{D} + {}^3\text{He}}{\text{H}}\right)_{\odot} = (4.1 \pm 0.6 \pm 1.4) \times 10^{-5} \quad (51)$$

The high temperature components in meteorites are believed to yield the true solar ${}^3\text{He}/\text{H}$ ratio of^{30,31}

$$\left(\frac{{}^3\text{He}}{\text{H}}\right)_{\odot} = (1.5 \pm 0.2 \pm 0.3) \times 10^{-5} \quad (52)$$

The difference between these two abundances reveals the presolar D/H ratio, giving,

$$(\text{D}/\text{H})_{\odot} \approx (2.6 \pm 0.6 \pm 1.4) \times 10^{-5} \quad (53)$$

It should be noted that recent measurements of surface abundances of HD on Jupiter show a somewhat higher value for D/H, $\text{D}/\text{H} = 5 \pm 2 \times 10^{-5}$ ³². If this value is confirmed and if fractionation does not significantly alter the D/H ratio (as it was suspected to for previous measurements involving CH_3D), it may have an important impact on galactic chemical evolution models. This value is marginally consistent with the inferred meteoritic values.

Finally, there have been several recent reported measurements of D/H in high redshift quasar absorption systems. Such measurements are in principle capable of determining the primordial value for D/H and hence η , because of the strong and monotonic dependence of D/H on η . However, at present, detections of D/H using quasar absorption systems do not yield a conclusive value for D/H. As such, it should be cautioned that these values may not turn out to represent the true primordial value and it is very unlikely that both are primordial and indicate an inhomogeneity³³. The first of these measurements³⁴ indicated a rather high D/H ratio, $\text{D}/\text{H} \approx 1.9 - 2.5 \times 10^{-4}$. Other high D/H ratios were reported in³⁵. However, there are reported low values of D/H in other such systems³⁶ with values $\text{D}/\text{H} \simeq 2.5 \times 10^{-5}$, significantly lower than the ones quoted above. Though this primordial D/H value is consistent with the solar and present values of D/H, it is not consistent (at the 2σ level) with the determinations of D/H in Jupiter, if they are correct. It is generally regarded that the high D/H measurements are of lesser quality while a recent observation³⁷ of the hydrogen column density in one of low D/H clouds found a significantly lower value and claimed a lower limit on D/H of 4×10^{-5} .

The range of quasar absorber D/H is shown by the dashed box in Figure 4. It is probably premature to use either of these values as the primordial

D/H abundance in an analysis of big bang nucleosynthesis, but it is certainly encouraging that future observations may soon yield a firm value for D/H. It is however important to note that there does seem to be a trend that over the history of the Galaxy, the D/H ratio is decreasing, something we expect from galactic chemical evolution. Of course the total amount of deuterium astration that has occurred is still uncertain, and model dependent.

There are also several types of ^3He measurements. As noted above, meteoritic extractions yield a presolar value for $^3\text{He}/\text{H}$ as given in Eq. (52). In addition, there are several ISM measurements of ^3He in galactic HII regions³⁸ which show a wide dispersion which may be indicative of pollution or a bias³⁹

$$\left(\frac{^3\text{He}}{\text{H}}\right)_{\text{HII}} \simeq 1 - 5 \times 10^{-5} \quad (54)$$

There is also a recent ISM measurement of ^3He ⁴⁰ with

$$\left(\frac{^3\text{He}}{\text{H}}\right)_{\text{ISM}} = 2.1^{+.9}_{-.8} \times 10^{-5} \quad (55)$$

Finally there are observations of ^3He in planetary nebulae⁴¹ which show a very high ^3He abundance of $^3\text{He}/\text{H} \sim 10^{-3}$.

Each of the light element isotopes can be made consistent with theory for a specific range in η . Overall consistency of course requires that the range in η agree among all four light elements. However, as will be argued below D and ^3He are far more sensitive to chemical evolution than ^4He or ^7Li and as such the direct comparison between the theoretical predictions of the primordial abundances of D and ^3He with the observational determination of their abundances is far more difficult. Therefore in what follows I will for the most part restrict the comparison between theory and observation to the two isotopes who suffer the least from the effects of chemical evolution.

2.2 Chemical Evolution

Because we can not directly measure the primordial abundances of any of the light element isotopes, we are required to make some assumptions concerning the evolution of these isotopes. As has been discussed above, ^4He is produced in stars along with oxygen and nitrogen. ^7Li can be destroyed in stars and produced in several (though still uncertain) environments. D is totally destroyed in the star formation process and ^3He is both produced and destroyed in stars with fairly uncertain yields. It is therefore preferable, if possible to observe the light element isotopes in a low metallicity environment. Such is the case with ^4He and ^7Li , and we can be fairly assured that the abundance determinations

of these isotopes are close to primordial. If the quasar absorption system measurements of D/H stabilize, then this too may be very close to a primordial measurement. Otherwise, to match the solar and present abundances of D and ^3He to their primordial values requires a model of galactic chemical evolution.

The main inputs to chemical evolution models are: 1) The initial mass function, $\phi(m)$, indicating the distribution of stellar masses. Typically, a simple power law form for the IMF is chosen, $\phi(m) \sim m^{-x}$, with $x \simeq -2.7$. This is a fairly good representation of the observed distribution, particularly at larger masses. 2) the star formation rate, ψ . Typical choices for a SFR are $\psi(t) \propto \sigma$ or σ^2 or even a straight exponential $e^{-t/\tau}$. σ is just the fraction of mass in gas, $M_{\text{gas}}/M_{\text{tot}}$. 3) the presence of infalling or outflowing gas; and of course 4) the stellar yields. It is the latter, particularly in the case of ^3He , that is the cause for so much uncertainty. Chemical evolution models simply set up a series of evolution equations which trace desired quantities. For example, σ and hence the SFR evolve through a relation such as

$$\frac{dM_{\text{gas}}}{dt} = -\psi(t) + e(t) + i(t) - o(t) \quad (56)$$

where e represents the amount of gas ejected from stars, i is the gas infall rate, and o is the gas outflow rate. Similar equations can be developed which trace the abundances of the element isotopes⁴².

Deuterium is always a monotonically decreasing function of time in chemical evolution models. The degree to which D is destroyed, is however a model dependent question which depends sensitively on the IMF and SFR. The evolution of ^3He is however considerably more complicated. Stellar models predict that substantial amounts of ^3He are produced in stars between 1 and 3 M_{\odot} . For $M < 8M_{\odot}$, Iben and Truran⁴³ calculate

$$(^3\text{He}/\text{H})_f = 1.8 \times 10^{-4} \left(\frac{M_{\odot}}{M} \right)^2 + 0.7 [(D + ^3\text{He})/\text{H}]_i \quad (57)$$

so that for example, when $\eta_{10} = 3$, $((D + ^3\text{He})/\text{H})_i = 9 \times 10^{-5}$, and the ratio of the final abundance of $^3\text{He}/\text{H}$ to the initial $(D + ^3\text{He})/\text{H}$ abundance denoted by g_3 is $g_3(1M_{\odot}) = 2.7$. The ^3He abundance is nearly tripled. It should be emphasized that this prediction is in fact consistent with the observation of high $^3\text{He}/\text{H}$ in planetary nebulae⁴¹.

Generally, implementation of the ^3He yield in Eq. (57) in chemical evolution models leads to an overproduction of $^3\text{He}/\text{H}$ particularly at the solar epoch^{39,44}. This problem is compounded in models with an intense period of D destruction. In Scully et al.⁴⁵, a dynamically generated supernovae wind model was coupled to models of galactic chemical evolution with the aim of reducing

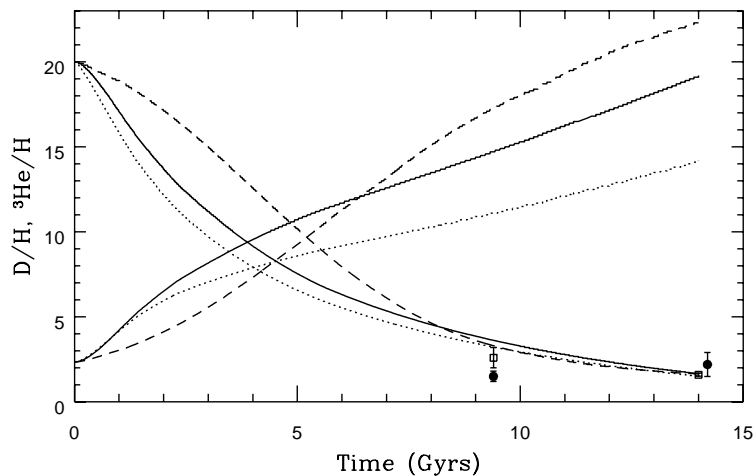


Figure 13: The evolution of D/H and ${}^3\text{He}/H$ with time in units of 10^{-5} .

a primordial D/H abundance of 2×10^{-4} to the present ISM value without overproducing heavy elements and remaining within the other observational constraints typically imposed on such models. In Figure 13, the evolution of D/H and ${}^3\text{He}/H$ is shown as a function of time in several representative models with significant deuterium destruction factors (see ref 45. for details). However, as one can plainly see, ${}^3\text{He}$ is grossly overproduced (the deuterium data is represented by squares and ${}^3\text{He}$ by circles).

The overproduction of ${}^3\text{He}$ relative to the solar meteoritic value seems to be a generic feature of chemical evolution models when ${}^3\text{He}$ production in low mass stars is included. This result appears to be independent of the chemical evolution model and is directly related to the assumed stellar yields of ${}^3\text{He}$. It has recently been suggested that at least some low mass stars may indeed be net destroyers of ${}^3\text{He}$ if one includes the effects of rotational mixing in low mass stars on the red giant branch^{46,47}. The extra mixing does not take place for stars which do not undergo a helium core flash (i.e. stars $> 1.7 - 2 M_{\odot}$). Thus stars with masses *less than* $1.7 M_{\odot}$ are responsible for the ${}^3\text{He}$ destruction. Using the yields of Boothroyd and Malaney⁴⁷, it was shown⁴⁸ that these reduced ${}^3\text{He}$ yields in low mass stars can account for the relatively low solar and present day ${}^3\text{He}/H$ abundances observed. In fact, in some cases,

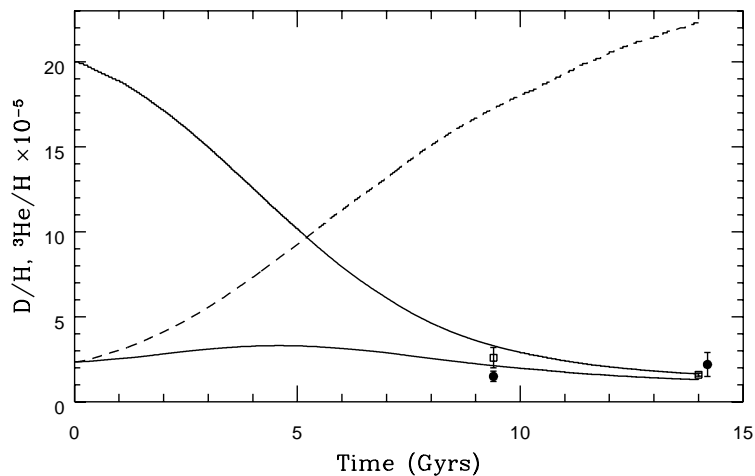


Figure 14: The evolution of D/H and ${}^3\text{He}/\text{H}$ with time using the reduced ${}^3\text{He}$ yields of ref. 47. The dashed curve is the same as in Figure 13, using standard ${}^3\text{He}$ yields.

${}^3\text{He}$ was underproduced. To account for the ${}^3\text{He}$ evolution and the fact that some low mass stars must be producers of ${}^3\text{He}$ as indicated by the planetary nebulae data, it was suggested that the new yields apply only to a fraction (albeit large) of low mass stars^{48,49}. The corresponding evolution⁴⁸ of D/H and ${}^3\text{He}/\text{H}$ is shown in Figure 14.

2.3 Likelihood Analysis

Monte Carlo techniques have proven to be a useful form of analysis for big bang nucleosynthesis^{50,51,14}. An analysis of this sort was performed¹⁰ using only ${}^4\text{He}$ and ${}^7\text{Li}$. It should be noted that in principle, two elements should be sufficient for not only constraining the one parameter (η) theory of BBN, but also for testing for consistency. The procedure begins by establishing likelihood functions for the theory and observations. For example, for ${}^4\text{He}$, the theoretical likelihood function takes the form

$$L_{\text{BBN}}(Y, Y_{\text{BBN}}) = e^{-(Y - Y_{\text{BBN}}(\eta))^2 / 2\sigma_1^2} \quad (58)$$

where $Y_{\text{BBN}}(\eta)$ is the central value for the ${}^4\text{He}$ mass fraction produced in the big bang as predicted by the theory at a given value of η , and σ_1 is the uncertainty

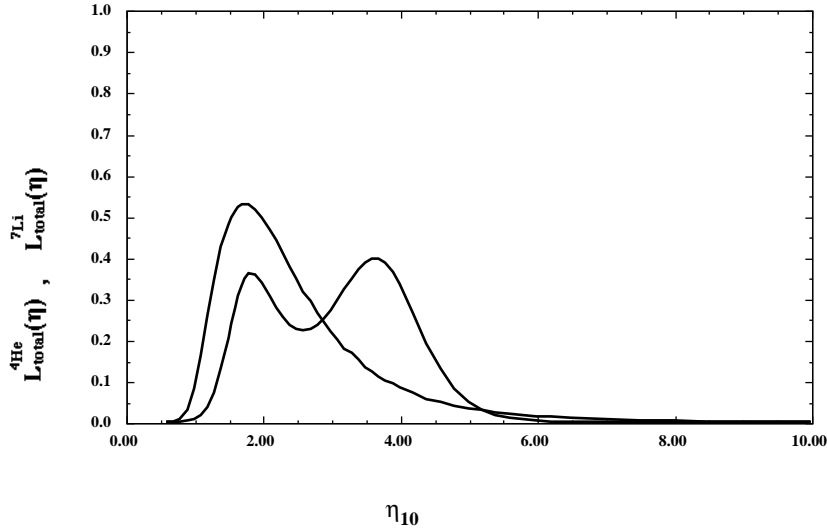


Figure 15: Likelihood distribution for each of ${}^4\text{He}$ and ${}^7\text{Li}$, shown as a function of η . The one-peak structure of the ${}^4\text{He}$ curve corresponds to its monotonic increase with η , while the two peaks for ${}^7\text{Li}$ arise from its passing through a minimum.

in that value derived from the Monte Carlo calculations¹⁴ and is a measure of the theoretical uncertainty in the big bang calculation. Similarly one can write down an expression for the observational likelihood function. Assuming Gaussian errors, the likelihood function for the observations would take a form similar to that in (58).

A total likelihood function for each value of η is derived by convolving the theoretical and observational distributions, which for ${}^4\text{He}$ is given by

$$L^{{}^4\text{He}}_{\text{total}}(\eta) = \int dY L_{\text{BBN}}(Y, Y_{\text{BBN}}(\eta)) L_{\text{O}}(Y, Y_{\text{O}}) \quad (59)$$

An analogous calculation is performed¹⁰ for ${}^7\text{Li}$. The resulting likelihood functions from the observed abundances given in Eqs. (48) and (49) is shown in Figure 15. As one can see there is very good agreement between ${}^4\text{He}$ and ${}^7\text{Li}$ in the vicinity of $\eta_{10} \simeq 1.8$. The double peaked nature of the ${}^7\text{Li}$ likelihood function is due to the presence of a minimum in the predicted lithium abundance. For a given observed value of ${}^7\text{Li}$, there are two likely values of η .

The combined likelihood, for fitting both elements simultaneously, is given by the product of the two functions in Figure 15 and is shown in Figure 16.

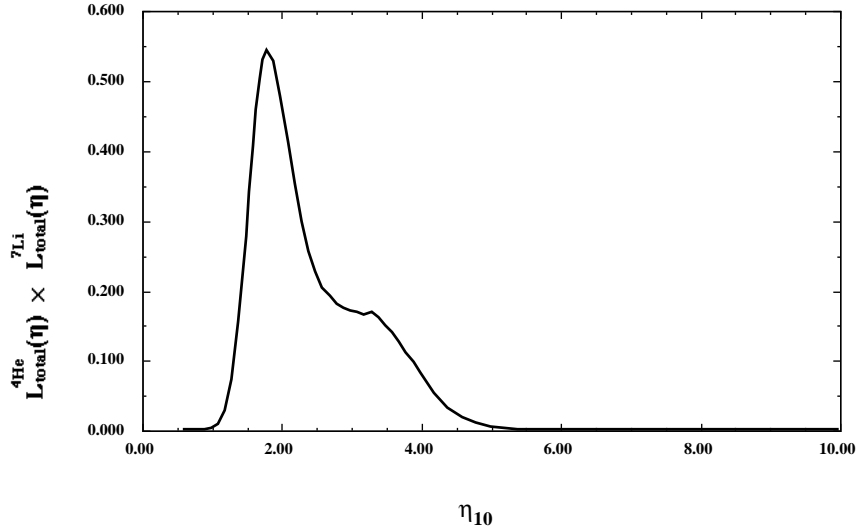


Figure 16: Combined likelihood for simultaneously fitting ${}^4\text{He}$ and ${}^7\text{Li}$, as a function of η .

From Figure 15 it is clear that ${}^4\text{He}$ overlaps the lower (in η) ${}^7\text{Li}$ peak, and so one expects that there will be concordance in an allowed range of η given by the overlap region. This is what one finds in Figure 16, which does show concordance and gives a preferred value for η , $\eta_{10} = 1.8_{-0.2}^{+1.2}$ corresponding to

$$\Omega_B h^2 = .006_{-.001}^{+.004} \quad (60)$$

Thus, we can conclude that the abundances of ${}^4\text{He}$ and ${}^7\text{Li}$ are consistent, and select an η_{10} range which overlaps with (at the 95% CL) the longstanding favorite range around $\eta_{10} = 3$. Furthermore, by finding concordance using only ${}^4\text{He}$ and ${}^7\text{Li}$, we deduce that if there is problem with BBN, it must arise from D and ${}^3\text{He}$ and is thus tied to chemical evolution or the stellar evolution of ${}^3\text{He}$. The most model-independent conclusion is that standard BBN with $N_\nu = 3$ is not in jeopardy. It is interesting to note that the central (and strongly) peaked value of η_{10} determined from the combined ${}^4\text{He}$ and ${}^7\text{Li}$ likelihoods is at $\eta_{10} = 1.8$. The corresponding value of D/H is 1.8×10^{-4} , very close⁵² to the high value of D/H in quasar absorbers^{34,35}. This is one of the main motivations for studying galactic chemical evolution models with high initial D/H and strong D destruction histories. Correspondingly, the the use

of reduced ${}^3\text{He}$ yields is essential as described in the previous section. Since D and ${}^3\text{He}$ are monotonic functions of η , a prediction for η , based on ${}^4\text{He}$ and ${}^7\text{Li}$, can be turned into a prediction for D and ${}^3\text{He}$. The corresponding 95% CL ranges are $\text{D}/\text{H} = (4.7 - 28) \times 10^{-5}$ and ${}^3\text{He}/\text{H} = (1.3 - 2.7) \times 10^{-5}$.

If we did have full confidence in the measured value of D/H in quasar absorption systems, then we could perform the same statistical analysis using ${}^4\text{He}$, ${}^7\text{Li}$, and D. To include D/H, one would proceed in much the same way as with the other two light elements. We compute likelihood functions for the BBN predictions as in Eq. (58) and the likelihood function for the observations using $\text{D}/\text{H} = (1.9 \pm 0.4) \times 10^{-4}$ i.e., using only the high value of D/H here. These are then convolved as in Eq. (59). In Figure 17, the resulting normalized distribution, $L_{\text{total}}^{\text{D}}(\eta)$ is super-imposed on distributions appearing in Figure 15. It is indeed startling how the three peaks, for D, ${}^4\text{He}$ and ${}^7\text{Li}$ are literally on top of each other. In Figure 18, the combined distribution is shown. We now have a very clean distribution and prediction for η , $\eta_{10} = 1.75_{-0.1}^{+0.4}$ corresponding to $\Omega_B h^2 = .006_{-0.0004}^{+0.001}$, with the peak of the distribution at $\eta_{10} = 1.75$. The absence of any overlap with the high- η peak of the ${}^7\text{Li}$ distribution has considerably lowered the upper limit to η . Overall, the concordance limits in this case are dominated by the deuterium likelihood function.

For the most part I have concentrated on the high D/H measurements in the likelihood analysis. If instead, we assume that the low value³⁶ of $\text{D}/\text{H} = (2.5 \pm 0.5) \times 10^{-5}$ is the primordial abundance, then we can again compare the likelihood distributions as in Figure 17, now substituting the low D/H value. As one can see from Figure 19, there is now hardly any overlap between the D and the ${}^7\text{Li}$ distributions and essentially no overlap with the ${}^4\text{He}$ distribution. The combined distribution shown in Figure 20 is compared with that in Figure 18. Though one can not use this likelihood analysis to prove the correctness of the high D/H measurements or the incorrectness of the low D/H measurements, the analysis clearly shows the difference in compatibility between the two values of D/H and the observational determinations of ${}^4\text{He}$ and ${}^7\text{Li}$. To *make* the low D/H measurement compatible, one would have to argue for a shift upwards in ${}^4\text{He}$ to a primordial value of 0.249 (a shift by 0.015) which is certainly not warranted at this time by the data, and a ${}^7\text{Li}$ depletion factor of about 3, which exceeds recent upper limits to the amount of depletion⁵³.

The implications of the resulting predictions from big bang nucleosynthesis on dark matter are clear. First, if $\Omega = 1$ (as predicted by inflation), and

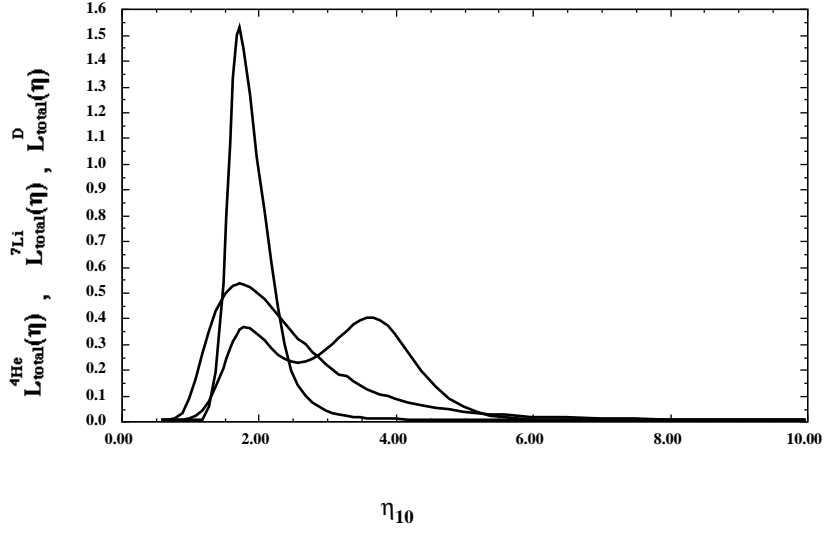


Figure 17: As in Figure 16, with the addition of the likelihood distribution for D/H.

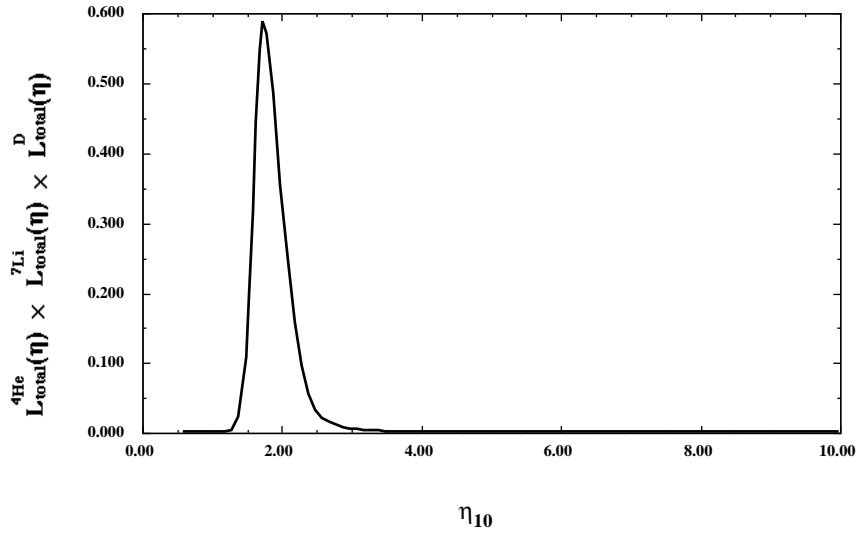


Figure 18: Combined likelihood for simultaneously fitting ${}^4\text{He}$ and ${}^7\text{Li}$, and D as a function of η .

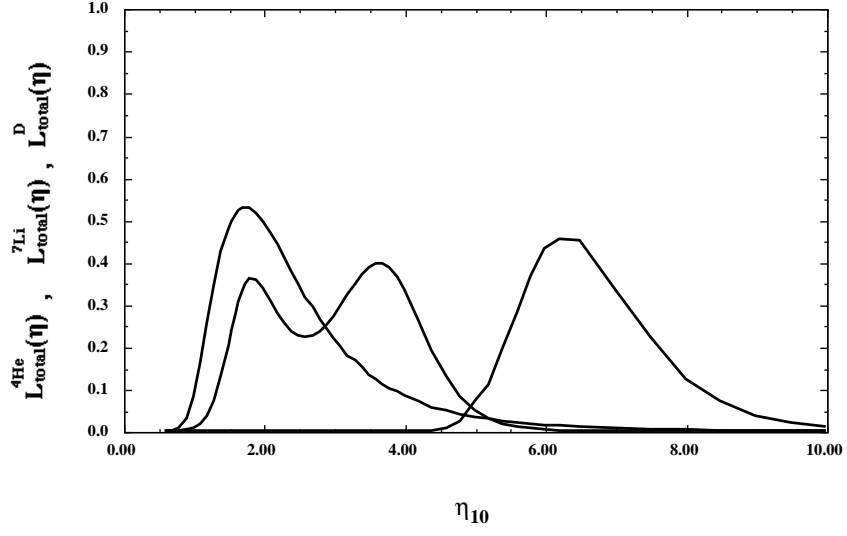


Figure 19: As in Figure 17, with the likelihood distribution for low D/H.

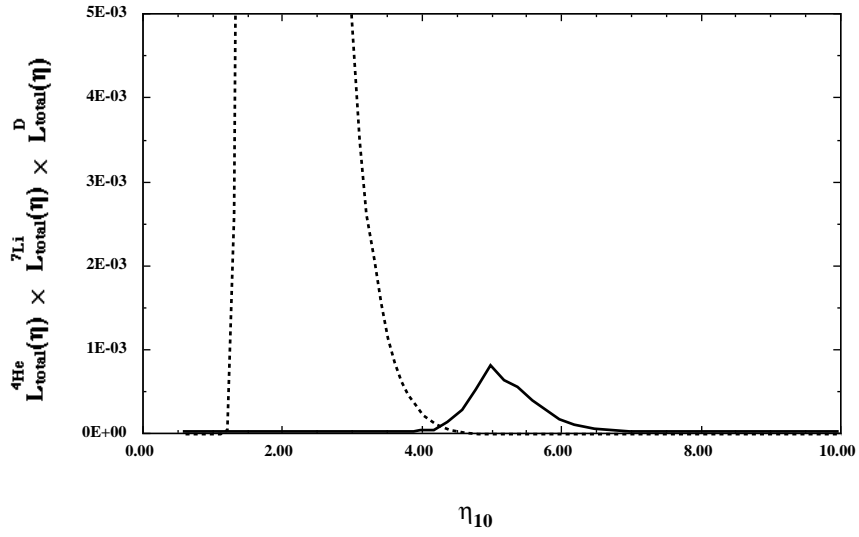


Figure 20: Combined likelihood for simultaneously fitting ${}^4\text{He}$ and ${}^7\text{Li}$, and low D/H as a function of η . The dashed curve represents the combined distribution shown in Figure 18.

$\Omega_B \lesssim 0.1$ which is certainly a robust conclusion based on D/H, then non-baryonic dark matter is a necessity. Second, on the scale of small groups of galaxies, $\Omega \gtrsim 0.05$, and is expected to sample the dark matter in galactic halos. This value is probably larger than the best estimate for Ω_B from equation (60). $\Omega_B h^2 = 0.0065$ corresponds to $\Omega_B = 0.025$ for $h = 1/2$. In this event, some non-baryonic dark matter in galactic halos is required. This conclusion is unchanged by the inclusion of the high D/H measurements in QSO absorbers. In contrast⁵⁴, the low D/H measurements would imply that $\Omega_B h^2 = 0.023$ allowing for the possibility that $\Omega_B \simeq 0.1$. In this case, no non-baryonic dark matter is required in galactic halos. However, I remind the reader that the low D/H is at present not consistent with either the observations of ${}^4\text{He}$ nor ${}^7\text{Li}$ and their interpretations as being primordial abundances. I will return to the subject of dark matter in the next lecture.

2.4 Constraints from BBN

Limits on particle physics beyond the standard model are mostly sensitive to the bounds imposed on the ${}^4\text{He}$ abundance. As is well known, the ${}^4\text{He}$ abundance is predominantly determined by the neutron-to-proton ratio just prior to nucleosynthesis and is easily estimated assuming that all neutrons are incorporated into ${}^4\text{He}$ (see Eq. (46)). As discussed earlier, the neutron-to-proton ratio is fixed by its equilibrium value at the freeze-out of the weak interaction rates at a temperature $T_f \sim 1$ MeV modulo the occasional free neutron decay. Furthermore, freeze-out is determined by the competition between the weak interaction rates and the expansion rate of the Universe

$$G_F^2 T_f^5 \sim \Gamma_{\text{wk}}(T_f) = H(T_f) \sim \sqrt{G_N N} T_f^2 \quad (61)$$

where N counts the total (equivalent) number of relativistic particle species. The presence of additional neutrino flavors (or any other relativistic species) at the time of nucleosynthesis increases the overall energy density of the Universe and hence the expansion rate leading to a larger value of T_f , (n/p), and ultimately Y_p . Because of the form of Eq. (61) it is clear that just as one can place limits⁵⁵ on N , any changes in the weak or gravitational coupling constants can be similarly constrained (for a recent discussion see ref. 56). In concluding this lecture, I will discuss the current constraint on N_ν the number of particle species (in neutrino units) and the limit on the strength of new interactions, if 3 right-handed (nearly massless) neutrinos are assumed to exist.

In the past, ${}^3\text{He}$ (together with D) has stood out in its importance for BBN, because it provided a (relatively large) lower limit for the baryon-to-photon ratio⁵⁷, $\eta_{10} > 2.8$. This limit for a long time was seen to be essential because it provided the only means for bounding η from below and in effect allows one to set an upper limit on the number of neutrino flavors⁵⁵, N_ν , as well as other constraints on particle physics properties. That is, the upper bound to N_ν is strongly dependent on the lower bound to η . This is easy to see: for lower η , the ${}^4\text{He}$ abundance drops, allowing for a larger N_ν , which would raise the ${}^4\text{He}$ abundance. However, for $\eta < 4 \times 10^{-11}$, corresponding to $\Omega_B h^2 \lesssim .001 - .002$, which is not too different from galactic mass densities, there is no bound whatsoever on N_ν ⁵⁸. Of course, with the improved data on ${}^7\text{Li}$, we do have lower bounds on η which exceed 10^{-10} .

Because, of new observations of D and ${}^3\text{He}$, and the new theoretical work on chemical evolution sparked by these observations, the bound on N_ν which is tied directly to these isotopes, should be called into question. As described earlier, the limits due to ${}^3\text{He}$ are ultimately tied to the assumed yields of low mass stars. Using the reduced yields as depicted in Figure 14, consistent values of $\eta < 2.8$ are certainly possible. Ultimately, as I have said repeatedly, D/H measurements in quasar absorption systems may soon resolve this issue. However, the lower values of η , relax the bounds on the number of neutrino flavors.

As discussed above, the limit on N_ν comes about via the change in the expansion rate given by the Hubble parameter,

$$H^2 = \frac{8\pi G}{3}\rho = \frac{8\pi^3 G}{90}[N_{\text{SM}} + \frac{7}{8}\Delta N_\nu]T^4 \quad (62)$$

when compared to the weak interaction rates. Here N_{SM} refers to the standard model value for N. At $T \sim 1$ MeV, $N_{\text{SM}} = 43/4$. Additional degrees of freedom will lead to an increase in the freeze-out temperature eventually leading to a higher ${}^4\text{He}$ abundance. In fact, one can parameterize the dependence of Y on N_ν by

$$Y = 0.2262 + 0.0131(N_\nu - 3) + 0.0135 \ln \eta_{10} \quad (63)$$

in vicinity of $\eta_{10} \sim 2$. Eq. (63) also shows the weak (log) dependence on η . However, rather than use (63) to obtain a limit, it is preferable to use the likelihood method.

Just as ${}^4\text{He}$ and ${}^7\text{Li}$ were sufficient to determine a value for η , a limit on N_ν can be obtained as well^{10,59}. The likelihood approach utilized above

can be extended to include N_ν as a free parameter. Since the light element abundances can be computed as functions of both η and N_ν , the likelihood function can be defined by⁵⁹

$$L_{\text{BBN}}(Y, Y_{\text{BBN}}) = e^{-(Y - Y_{\text{BBN}}(\eta, N_\nu))^2 / 2\sigma_1^2} \quad (64)$$

and

$$L^{4\text{He}}_{\text{total}}(\eta, N_\nu) = \int dY L_{\text{BBN}}(Y, Y_{\text{BBN}}(\eta, N_\nu)) L_{\text{O}}(Y, Y_{\text{O}}) \quad (65)$$

Again, similar expressions are needed for ${}^7\text{Li}$ and D. A three-dimensional view of the combined likelihood functions⁵⁹ is shown in Figure 21. In this case the high and low η maxima of Figure 15, show up as peaks in the $L - \eta - N_\nu$ space (L_{47} when D/H is neglected and L_{247} when D/H is included). The peaks of the distribution as well as the allowed ranges of η and N_ν are more easily discerned in the contour plot of Figure 22 which shows the 50%, 68% and 95% confidence level contours in the two likelihood functions. The crosses show the location of the peaks of the likelihood functions. L_{47} peaks at $N_\nu = 3.0$, $\eta_{10} = 1.8$ (in agreement with our previous results¹⁰) and at $N_\nu = 2.3$, $\eta_{10} = 3.6$. The 95% confidence level allows the following ranges in η and N_ν

$$1.6 \leq N_\nu \leq 4.0 \quad 1.3 \leq \eta_{10} \leq 5.0 \quad (66)$$

Note however that the ranges in η and N_ν are strongly correlated as is evident in Figure 22. Since the deuterium likelihood function picks out a small range of values of η , largely independent of N_ν , its effect on L_{247} is to eliminate one of the two peaks in L_{47} . L_{247} also peaks at $N_\nu = 3.0$, $\eta_{10} = 1.8$. In this case the 95% contour gives the ranges

$$2.0 \leq N_\nu \leq 4.1 \quad 1.4 \leq \eta_{10} \leq 2.6 \quad (67)$$

One should recall that the limit derived above is not meant for neutrinos in the strictest sense. That is, the limit is only useful when applied to additional particle degrees of freedom which necessarily do not couple to the Z^0 . For very weakly interacting particles, one must take into account the reduced abundance of these particles at the time of nucleosynthesis⁶⁰. As discussed in the first lecture, the number of neutrinos today is reduced relative to the number of photons by $(T_\nu/T_\gamma)^3 = 4/11$. For some new particle, χ , which decoupled at $T_d > 1$ MeV, the same argument based on the conservation of entropy tells us that

$$\left(\frac{T_\chi}{T_\gamma}\right)^3 = \frac{43}{4N(T_d)} \quad (68)$$

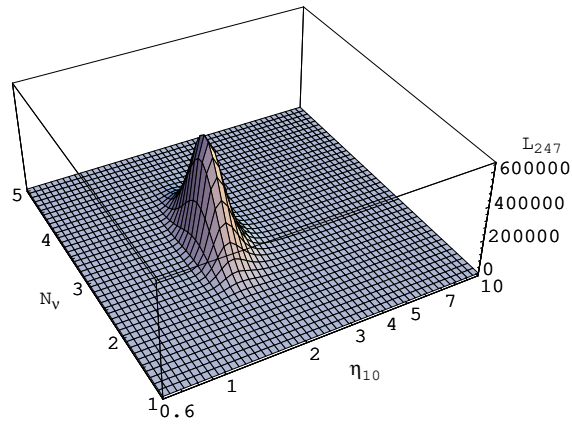
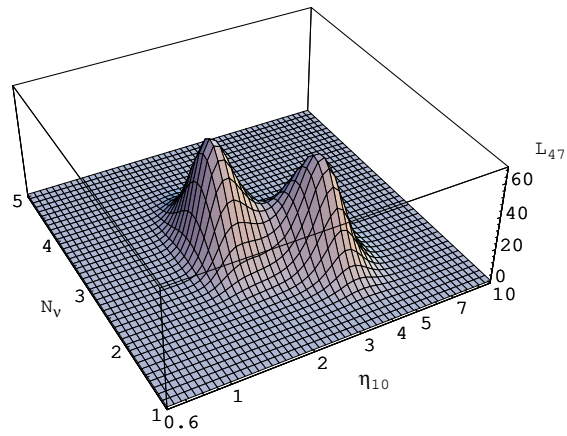


Figure 21: The combined two-dimensional likelihood functions for simultaneously fitting ${}^4\text{He}$ and ${}^7\text{Li}$ in the top panel, and including D in the lower one as functions of both η and N_{ν} .

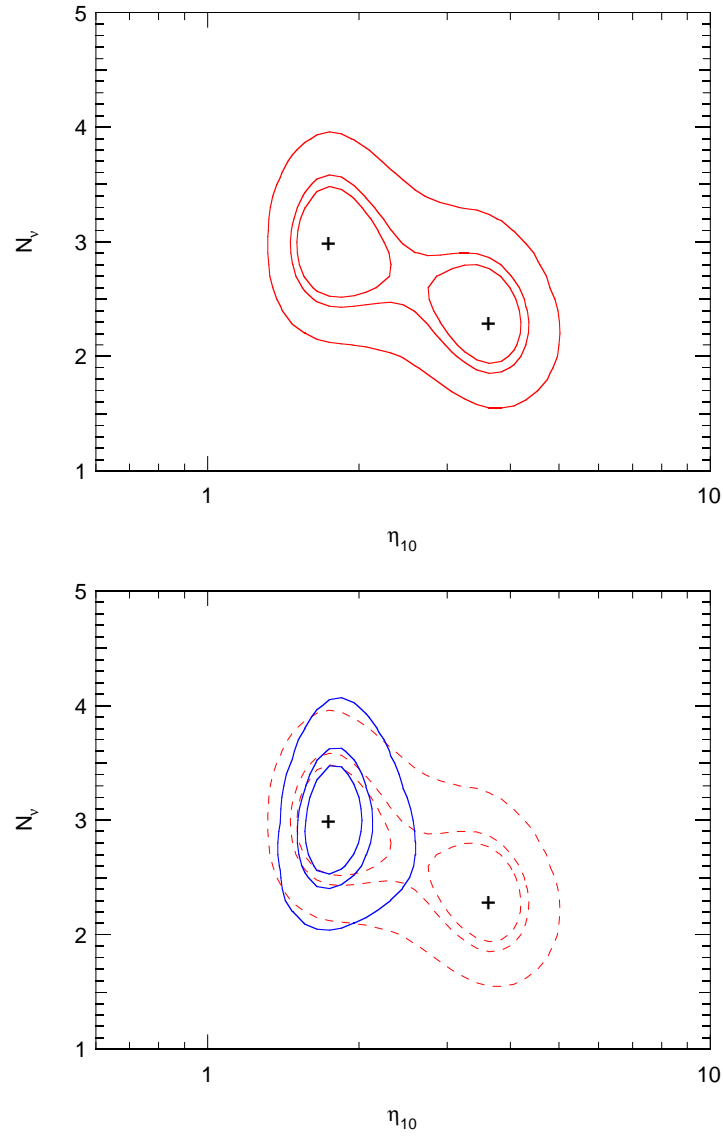


Figure 22: The top panel shows contours in the combined likelihood function for ${}^4\text{He}$ and ${}^7\text{Li}$. The contours represent 50% (innermost), 68% and 95% (outermost) confidence levels. The crosses mark the points of maximum likelihood. Also shown is the equivalent result when D is included.

Thus we can translate the bound on N_ν , which is really a bound on the additional energy density at nucleosynthesis

$$\Delta\rho = \frac{\pi^2}{30} \left[\sum g_B \left(\frac{T_B}{T}\right)^4 + \frac{7}{8} \sum g_F \left(\frac{T_F}{T}\right)^4 \right] T^4 \quad (69)$$

for additional boson states with g_B degrees of freedom and fermion states with g_F degrees of freedom. At nucleosynthesis $T = T_\nu = T_\gamma$ and the limit $N_\nu < 4$ becomes

$$\frac{8}{7} \sum \frac{g_B}{2} \left(\frac{T_B}{T_\nu}\right)^4 + \sum \frac{g_F}{2} \left(\frac{T_F}{T}\right)^4 < 1 \quad (70)$$

Such a limit would allow a single additional scalar degree of freedom (which counts as $\frac{4}{7}$) such as a majoron. On the other hand, in models with right-handed interactions, and three right-handed neutrinos, the constraint is severe. The right-handed states must have decoupled early enough to ensure $(T_{\nu_R}/T_{\nu_L})^4 < 1/3$. The temperature of a decoupled state is easily determined from (68). Three right-handed neutrinos would require $N(T_d) \gtrsim 25$, which from Figure 1 implies that $T_d > 140$ MeV, conservatively assuming a QCD transition temperature of 150 MeV. If right-handed interactions are mediated by additional gauge interactions, associated with some scale $M_{Z'}$, and if we assume that the right handed interactions scale as $M_{Z'}^4$, with a standard model-like coupling, then the decoupling temperature of the right handed interactions is related to $M_{Z'}$ by

$$\left(\frac{T_{dR}}{T_{dL}}\right)^3 \sim \left(\frac{M_{Z'}}{M_Z}\right)^4 \quad (71)$$

which for $T_{dL} \sim 3$ MeV (a more accurate value than the 1 MeV estimate) and $T_{dL} \gtrsim 140$ MeV, we find that the associated mass scale becomes $M_{Z'} \gtrsim 1.6$ TeV! In general this constraint is very sensitive to the BBN limit on N_ν . In Figure 23, the allowed number of neutrino degrees of freedom are shown as a function of their decoupling temperature for the case of $N_\nu < 4$ and $N_\nu < 3.3$, shown for comparison.

2.5 Summary

To summarize on the subject of big bang nucleosynthesis, I would assert that one can conclude that the present data on the abundances of the light element isotopes are consistent with the standard model of big bang nucleosynthesis. Using the the isotopes with the best data, ^4He and ^7Li , it is possible to constrain the theory and obtain a best value for the baryon-to-photon ratio of

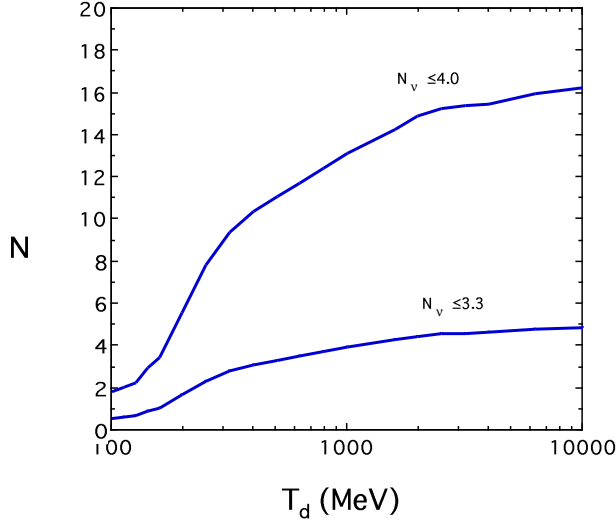


Figure 23: Limits on neutrino-like degrees of freedom.

$\eta_{10} = 1.8$, a corresponding value $\Omega_B h^2 = .0065$ and

$$\begin{aligned} 1.4 &< \eta_{10} < 4.2 && 95\%CL \\ .005 &< \Omega_B h^2 < .015 && 95\%CL \end{aligned} \quad (72)$$

For $0.4 < h < 1$, we have a range $.005 < \Omega_B < .10$. This is a rather low value for the baryon density and would suggest that much of the galactic dark matter is non-baryonic⁶¹. These predictions are in addition consistent with recent observations of D/H in quasar absorption systems which show a high value. Difficulty remains however, in matching the solar ^3He abundance, suggesting a problem with our current understanding of galactic chemical evolution or the stellar evolution of low mass stars as they pertain to ^3He .

3 Dark Matter

There is increasing evidence that relative to the visible matter in the Universe, which is in the form of baryons, there is considerably more matter in the Universe that we don't see⁶². Here, I will review some of the motivations for the existence of dark matter in the Universe. The best observational evidence is found on the scale of galactic halos and comes from the observed flat rotation

curves of galaxies. There is also mounting evidence for dark matter in elliptical galaxies, as well as clusters of galaxies coming from X-ray observations of these objects. Also, direct evidence has been obtained through the study of gravitational lenses. In theory, we believe there is much more matter because 1) inflation tells us so (and there is at present no good alternative to inflation) and 2) our current understanding of galaxy formation only makes sense if there is more matter than we see. One can also make a strong case for the existence of non-baryonic dark matter in particular. The recurrent problem with baryonic dark matter is that not only is it very difficult to hide baryons, but the standard model of primordial nucleosynthesis would have to be discarded if all of the dark matter is baryonic. Fortunately, as will be covered at length in these proceedings, there are several attractive alternatives to baryonic dark matter.

There is, in fact, good evidence for dark matter on the scale of galaxies (and their halos). Assuming that galaxies are in virial equilibrium, one expects that by Newton's Laws one can relate the mass at a given distance r , from the center of a galaxy to its rotational velocity

$$M(r) \propto v^2 r / G_N \quad (73)$$

The rotational velocity, v , is measured^{63,64,65} by observing 21 cm emission lines in HI regions (neutral hydrogen) beyond the point where most of the light in the galaxy ceases. A compilation of nearly 1000 rotation curves of spiral galaxies has been plotted in ref. 66 as a function of r for varying brightnesses. If the bulk of the mass is associated with light, then beyond the point where most of the light stops M would be constant and $v^2 \propto 1/r$. This is not the case, as the rotation curves appear to be flat, i.e., $v \sim \text{constant}$ outside the core of the galaxy. This implies that $M \propto r$ beyond the point where the light stops. This is one of the strongest pieces of evidence for the existence of dark matter. Velocity measurements indicate dark matter in elliptical galaxies as well⁶⁷.

Galactic rotation curves are not the only observational indication for the existence of dark matter. X-ray emitting hot gas in elliptical galaxies also provides an important piece of evidence for dark matter. As an example, consider the large elliptical M87. The detailed profiles of the temperature and density of the hot X-ray emitting gas have been mapped out⁶⁸. By assuming hydrostatic equilibrium, these measurements allow one to determine the overall mass distribution in the galaxy necessary to bind the hot gas. Based on an isothermal model with temperature $kT = 3\text{keV}$ (which leads to a conservative estimate of the total mass), Fabricant and Gorenstein⁶⁸ predicted that the

total mass out to a radial distance of 392 Kpc is $5.7 \times 10^{13} M_{\odot}$, whereas the mass in the hot gas is only $2.8 \times 10^{12} M_{\odot}$ or only 5% of the total. The visible mass is expected to contribute only 1% of the total. The inferred value of Ω based on M87 would be ~ 0.2 .

M87 is not the only example of an elliptical galaxy in which X-ray emitting hot gas is observed to indicate the presence of dark matter. In addition, similar inferences regarding the existence of dark matter can be made from the X-ray emission from small groups of galaxies^{69,70}.

On very large scales, it is possible to get an estimate of Ω from the distribution of peculiar velocities. On scales, λ , where perturbations, δ , are still small, peculiar velocities can be expressed⁷¹ as $v \sim H\lambda\delta\Omega^{0.6}$. On these scales, older measurements of the peculiar velocity field from the IRAS galaxy catalogue indicate that indeed Ω is close to unity⁷². Some of the new data⁷³ indicates perhaps a lower value in range 0.2 – 0.5, but does not conclusively exclude $\Omega = 1$. Another piece of evidence on large scales is available from gravitational lensing⁷⁴. The systematic lensing of the roughly 150,000 galaxies per deg² at redshifts between $z = 1 - 3$ into arcs and arclets allow one to trace the matter distribution in a foreground cluster. Unfortunately, none of these observations reveal the identity of the dark matter.

Theoretically, there is no lack of support for the dark matter hypothesis. The standard big bang model including inflation almost requires that $\Omega = 1$ ⁸. If this is the case and $\Omega = 1$, then we know two things: Dark matter exists, since we don't see $\Omega = 1$ in luminous objects, and most (at least 90%) of the dark matter is not baryonic. The latter conclusion is a result of our previous discussion on BBN which constrains the baryon-to-photon ratio and hence Ω_B as in eq. (72). Thus $1 - \Omega_B$ is not only dark but also non-baryonic.

Another important piece of theoretical evidence for dark matter comes from the simple fact that we are here living in a galaxy. The type of perturbations produced by inflation⁷⁵ are, in most models, adiabatic perturbations ($\delta\rho/\rho \propto \delta T/T$), and I will restrict my attention to these. Indeed, the perturbations produced by inflation also have the very nearly scale-free spectrum described by Harrison and Zeldovich⁷⁶. When produced, scale-free perturbations fall off as $\frac{\delta\rho}{\rho} \propto l^{-2}$ (increase as the square of the wave number). At early times $\delta\rho/\rho$ grows as t until the time when the horizon scale (which is proportional to the age of the Universe) is comparable to l . At later times, the growth halts (the mass contained within the volume l^3 has become smaller than the Jean's mass) and $\frac{\delta\rho}{\rho} = \delta$ (roughly) independent of the scale l . When

the Universe becomes matter dominated, the Jean's mass drops dramatically and growth continues as $\frac{\delta\rho}{\rho} \propto R \sim 1/T$.

The transition to matter dominance is determined by setting the energy densities in radiation (photons and any massless neutrinos) equal to the energy density in matter (baryons and any dark matter). For three massless neutrinos and baryons (no dark matter), matter dominance begins at

$$T_m = 0.22m_B\eta \quad (74)$$

and for $\eta < 3.8 \times 10^{-10}$, this corresponds to $T_m < 0.08$ eV.

Because we are considering adiabatic perturbations, there will be anisotropies produced in the microwave background radiation on the order of $\delta T/T \sim \delta$. The value of δ , the amplitude of the density fluctuations at horizon crossing, has now been determined by COBE⁷⁷, $\delta = (5.7 \pm 0.4) \times 10^{-6}$. Without the existence of dark matter, $\delta\rho/\rho$ in baryons could then achieve a maximum value of only $\delta\rho/\rho \sim A_\lambda\delta(T_m/T_o) \lesssim 2 \times 10^{-3}A_\lambda$, where $T_o = 2.35 \times 10^{-4}$ eV is the present temperature of the microwave background and $A_\lambda \sim 1 - 10$ is a scale dependent growth factor. The overall growth in $\delta\rho/\rho$ is too small to argue that growth has entered a nonlinear regime needed to explain the large value (10^5) of $\delta\rho/\rho$ in galaxies.

Dark matter easily remedies this dilemma in the following way. The transition to matter dominance is determined by setting equal to each other the energy densities in radiation (photons and any massless neutrinos) and matter (baryons and any dark matter). While if we suppose that there exists dark matter with an abundance $Y_\chi = n_\chi/n_\gamma$ (the ratio of the number density of χ 's to photons) then

$$T_m = 0.22m_\chi Y_\chi \quad (75)$$

Since we can write $m_\chi Y_\chi/\text{GeV} = \Omega_\chi h^2/(4 \times 10^7)$, we have $T_m/T_o = 2.4 \times 10^4 \Omega_\chi h^2$ which is to be compared with 350 in the case of baryons alone. The baryons, although still bound to the radiation until decoupling, now see deep potential wells formed by the dark matter perturbations to fall into and are no longer required to grow at the rate $\delta\rho/\rho \propto R$.

With regard to dark matter and galaxy formation, all forms of dark matter are not equal. They can be distinguished by their relative temperature at T_m ⁷⁸. Particles which are still largely relativistic at T_m (like neutrinos or other particles with $m_\chi < 100$ eV) have the property⁷⁹ that (due to free streaming)

they erase perturbations out to very large scales given by the Jean's mass

$$M_J = 3 \times 10^{18} \frac{M_\odot}{m_\chi^2(\text{eV})} \quad (76)$$

Thus, very large scale structures form first and galaxies are expected to fragment out later. Particles with this property are termed hot dark matter particles. Cold particles ($m_\chi > 1$ MeV) have the opposite behavior. Small scale structure forms first aggregating to form larger structures later. Neither candidate is completely satisfactory when the resulting structure is compared to the observations. For more details, I refer the reader to reviews in refs. 62.

Accepting the dark matter hypothesis, the first choice for a candidate should be something we know to exist, baryons. Though baryonic dark matter can not be the whole story if $\Omega = 1$, the identity of the dark matter in galactic halos, which appear to contribute at the level of $\Omega \sim 0.05$, remains an important question needing to be resolved. A baryon density of this magnitude is not excluded by nucleosynthesis. Indeed we know some of the baryons are dark since $\Omega \lesssim 0.01$ in the disk of the galaxy.

It is quite difficult, however, to hide large amounts of baryonic matter⁸⁰. Sites for halo baryons that have been discussed include snowballs, which tend to sublimate, cold hydrogen gas, which must be supported against collapse, and hot gas, which can be excluded by the X-ray background. Stellar objects (collectively called MACHOs for macroscopic compact halo objects) must either be so small ($M < 0.08 M_\odot$) so as not to have begun nuclear burning or so massive so as to have undergone total gravitational collapse without the ejection of heavy elements. Intermediate mass stars are generally quite problematic because either they are expected to still reside on the main-sequence today and hence would be visible, or they would have produced an excess of heavy elements.

On the other hand, MACHOs are a candidate which are testable by the gravitational microlensing of stars in a neighboring galaxy such as the LMC⁸¹. By observing millions of stars and examining their intensity as a function of time, it may be possible to determine the presence of dark objects in our halo. It is expected that during a lensing event, a star in the LMC will have its intensity rise in an achromatic fashion over a period $\delta t \sim 3 \sqrt{M/.001M_\odot}$ days. Indeed, microlensing candidates have been found⁸². For low mass objects, those with $M < 0.1M_\odot$, it appears however that the halo fraction of MACHOs is small, $\approx 0.19_{-0.10}^{+0.16}$ ⁸³. Recent results from the MACHO collaboration⁸⁴ show events with longer duration comprising about half the halo, leading to the

speculation of a white dwarf population in the halo. Though it is too early to determine the implications of these observations, they are very encouraging in that perhaps this issue can and will be decided.

If we now take as given that non-baryonic dark matter is required, we are faced with the problem of its identity. Light neutrinos ($m \leq 30eV$) are a long-time standard when it comes to non-baryonic dark matter⁸⁵. Light neutrinos produce structure on large scales, and the natural (minimal) scale for structure clustering is given in Eq. (76). Hence neutrinos offer the natural possibility for large scale structures^{86,87} including filaments and voids. It seemed, however, that neutrinos were ruled out because they tend to produce too much large scale structure⁸⁸. Because the smallest non-linear structures have mass scale M_J and the typical galactic mass scale is $\simeq 10^{12}M_\odot$, galaxies must fragment out of the larger pancake-like objects. The problem is that in such a scenario, galaxies form late^{87,89} ($z \leq 1$) whereas quasars and galaxies are seen out to redshifts $z \gtrsim 4$. Recently, neutrinos are seeing somewhat of a revival in popularity in mixed dark matter models.

In the standard model, the absence of a right-handed neutrino state precludes the existence of a neutrino mass. By adding a right-handed state ν_R , it is possible to generate a Dirac mass for the neutrino, $m_\nu = h_\nu v / \sqrt{2}$, as for the charged lepton masses, where h_ν is the neutrino Yukawa coupling constant, and v is the Higgs expectation value. It is also possible to generate a Majorana mass for the neutrino when in addition to the Dirac mass term, $m_\nu \bar{\nu}_R \nu_L$, a term $M \nu_R \nu_R$ is included. In what is known as the see-saw mechanism, the two mass eigenstates are given by $m_{\nu_1} \sim m_\nu^2 / M$ which is very light, and $m_{\nu_2} \sim M$ which is heavy. The state ν_1 is our hot dark matter candidate as ν_2 is in general not stable.

The cosmological constraint on the mass of a light neutrino is derived from the overall mass density of the Universe. In general, the mass density of a light particle χ can be expressed as

$$\rho_\chi = m_\chi Y_\chi n_\gamma \leq \rho_c = 1.06 \times 10^{-5} h_o^2 \text{GeV}/\text{cm}^3 \quad (77)$$

where $Y_\chi = n_\chi / n_\gamma$ is the density of χ 's relative to the density of photons, for $\Omega h_o^2 < 1$. For neutrinos $Y_\nu = 3/11$, and one finds⁹⁰

$$\sum_\nu \left(\frac{g_\nu}{2}\right) m_\nu < 93eV(\Omega h_o^2) \quad (78)$$

where the sum runs over neutrino flavors. All particles with abundances Y similar to neutrinos will have a mass limit given in Eq. (78).

It was possible that neutrinos (though not any of the known flavors) could have had large masses, $m_\nu > 1$ MeV. In that case their abundance Y is controlled by $\nu, \bar{\nu}$ annihilations⁹¹, for example, $\nu\bar{\nu} \rightarrow f\bar{f}$ via Z exchange. When the annihilations freeze-out (the annihilation rate becomes slower than the expansion rate of the Universe), Y becomes fixed. Roughly, $Y \sim (m\sigma_A)^{-1}$ and $\rho \sim \sigma_A^{-1}$ where σ_A is the annihilation cross-section. For neutrinos, we expect $\sigma_A \sim m_\nu^2/m_Z^4$ so that $\rho_\nu \sim 1/m_\nu^2$ and we can derive a lower bound^{91,92,93} on the neutrino mass, $m_\nu \gtrsim 3 - 7$ GeV, depending on whether it is a Dirac or Majorana neutrino. Indeed, any particle with roughly a weak scale cross-sections will tend to give an interesting value of $\Omega h^2 \sim 1$.

Due primarily to the limits from LEP⁹⁴, the heavy massive neutrino has become simply an example and is no longer a dark matter candidate. LEP excludes neutrinos (with standard weak interactions) with masses $m_\nu \lesssim 45$ GeV. Lab constraints for Dirac neutrinos are available⁹⁵, excluding neutrinos with masses between 10 GeV and 4.7 TeV. This is significant, since it precludes the possibility of neutrino dark matter based on an asymmetry between ν and $\bar{\nu}$ ⁹⁶. Majorana neutrinos are excluded as *dark matter* since $\Omega_\nu h_o^2 < 0.001$ for $m_\nu > 45$ GeV and are thus cosmologically uninteresting.

If we return to our example of right-handed neutrinos, we saw in the previous section on constraints from BBN that because right-handed interactions are weaker than standard left-handed interactions, they decouple early and today are at a reduced temperature relative to ν_L (cf. eq. (68)). As such, for $T_{dR} \gg 1$ MeV, $n_{\nu_R}/n_{\nu_L} = (T_{\nu_R}/T_{\nu_L})^3 \ll 1$. Thus the abundance of right-handed neutrinos can be written as

$$Y_{\nu_R} = \frac{n_{\nu_R}}{n_\gamma} = \left(\frac{3}{11}\right)\left(\frac{T_{\nu_R}}{T_{\nu_L}}\right)^3 \ll \frac{3}{11} \quad (79)$$

In this case, the previous bound (78) on neutrino masses is weakened. For a suitably large scale for the right-handed interactions, right-handed neutrino masses may be as large as a few keV⁹⁷.

Supersymmetric theories introduce several possible candidates. If R-parity, which distinguishes between “normal” matter and the supersymmetric partners and can be defined in terms of baryon, lepton and spin as $R = (-1)^{3B+L+2S}$, is unbroken, there is at least one supersymmetric particle which must be stable. I will assume R-parity conservation, which is common in the minimal supersymmetric standard model (MSSM). R-parity is generally assumed in order to justify the absence of superpotential terms which can be responsible for rapid proton decay. The stable particle (usually called the LSP) is most probably

some linear combination of the $R = -1$ neutral fermions, the neutralinos⁹⁸: the wino \tilde{W}^3 , the partner of the 3rd component of the $SU(2)_L$ gauge boson; the bino, \tilde{B} , the partner of the $U(1)_Y$ gauge boson; and the two neutral Higgsinos, \tilde{H}_1 and \tilde{H}_2 . Gluinos are expected to be heavier $-m_{\tilde{g}} = (\frac{\alpha_3}{\alpha}) \sin^2 \theta_W M_2$, where M_2 is the supersymmetry breaking $SU(2)$ gaugino mass— and they do not mix with the other states. The sneutrino⁹⁹ is also a possibility but has been excluded as a dark matter candidate by direct⁹⁵ searches, indirect¹⁰⁰ and accelerator⁹⁴ searches.

There are relatively few parameters in the minimal model and the identity of the LSP is determined by three:

1. M_2 ; if one assumes a common soft supersymmetry breaking gaugino mass at the unification scale in the Lagrangian, $\mathcal{L} \ni M_2 \tilde{W} \tilde{W}$.
2. μ ; a Higgs mixing mass, $\mathcal{L} \ni \mu \tilde{H}_1 \tilde{H}_2$ necessary to avoid phenomenologically unacceptable axions.
3. $\tan \beta$; the ratio of Higgs expectation values, $\tan \beta = \frac{v_1}{v_2}$, where $v_1 = \langle H_1 \rangle$, $v_2 = \langle H_2 \rangle$ is also a free parameter but can be chosen to be positive without loss of generality. In this notation, it is H_1 which is responsible for up quark masses so that it will be natural to assume $\tan \beta > 1$.

The LSP can be expressed as a linear combination

$$\chi = \alpha \tilde{W}^3 + \beta \tilde{B} + \gamma \tilde{H}_1 + \delta \tilde{H}_2 \quad (80)$$

Pure state LSP possibilities are : The photino¹⁰¹

$$\tilde{\gamma} = \tilde{W}^3 \sin \theta_W + \tilde{B} \cos \theta_W \quad (81)$$

the Higgsino, \tilde{S}^0 ⁹⁸

$$\tilde{S}^0 = \tilde{H}_1 \cos \beta + \tilde{H}_2 \sin \beta \quad (82)$$

the bino¹⁰²,

$$\tilde{B} = \tilde{B} \quad (83)$$

and the Higgsinos \tilde{H}_{12} ¹⁰²

$$\tilde{H}_{12} = \frac{1}{\sqrt{2}}(\tilde{H}_1 \pm \tilde{H}_2) \quad (84)$$

The solution for the coefficients α, β, γ and δ for neutralinos that make up the LSP can be found by diagonalizing the mass matrix

$$(\tilde{W}^3, \tilde{B}, \tilde{H}_1^0, \tilde{H}_2^0) \begin{pmatrix} M_2 & 0 & \frac{-g_2 v_1}{\sqrt{2}} & \frac{g_2 v_2}{\sqrt{2}} \\ 0 & M_1 & \frac{g_1 v_1}{\sqrt{2}} & \frac{-g_1 v_2}{\sqrt{2}} \\ \frac{-g_2 v_1}{\sqrt{2}} & \frac{g_1 v_1}{\sqrt{2}} & 0 & -\mu \\ \frac{g_2 v_2}{\sqrt{2}} & \frac{-g_1 v_2}{\sqrt{2}} & -\mu & 0 \end{pmatrix} \begin{pmatrix} \tilde{W}^3 \\ \tilde{B} \\ \tilde{H}_1^0 \\ \tilde{H}_2^0 \end{pmatrix} \quad (85)$$

where M_1 is a soft supersymmetry breaking term giving mass to the U(1) gaugino. In a unified theory $M_1 = M_2$ at the unification scale translates to

$$M_1 = \frac{5}{3} \frac{\alpha_1}{\alpha_2} M_2 \quad (86)$$

at low energies. By performing a change of basis to $\tilde{W}^3, \tilde{B}, \tilde{A}^0, \tilde{S}^0$ with

$$\tilde{A}^0 = \tilde{H}_1^0 \sin \beta - \tilde{H}_2^0 \cos \beta \quad (87)$$

the mass matrix simplifies and becomes

$$(\tilde{W}^3, \tilde{B}, \tilde{A}^0, \tilde{S}^0) \begin{pmatrix} M_2 & 0 & \frac{-g_2 v}{\sqrt{2}} & 0 \\ 0 & M_1 & \frac{g_1 v}{\sqrt{2}} & 0 \\ \frac{-g_2 v}{\sqrt{2}} & \frac{g_1 v}{\sqrt{2}} & \frac{2v_1 v_2}{v^2} \mu & \frac{v_2^2 - v_1^2}{v^2} \mu \\ 0 & 0 & \frac{v_2^2 - v_1^2}{v^2} \mu & \frac{-2v_1 v_2}{v^2} \mu \end{pmatrix} \begin{pmatrix} \tilde{W}^3 \\ \tilde{B} \\ \tilde{A}^0 \\ \tilde{S}^0 \end{pmatrix} \quad (88)$$

where $v^2 = v_1^2 + v_2^2$ and can be solved analytically. The lightest mass eigenstate is the LSP.

There are some limiting cases in which the LSP is nearly a pure state. When $\mu \rightarrow 0$, \tilde{S}^0 is the LSP with

$$m_{\tilde{S}} \rightarrow \frac{2v_1 v_2}{v^2} \mu \quad (89)$$

When $M_2 \rightarrow 0$, the photino is the LSP with

$$m_{\tilde{\gamma}} \rightarrow \frac{8}{3} \frac{g_1^2}{(g_1^2 + g_2^2)} M_2 \quad (90)$$

When M_2 is large and $M_2 \ll \mu$ then the bino \tilde{B} is the LSP and

$$m_{\tilde{B}} \simeq M_1 \quad (91)$$

and finally when μ is large and $\mu \ll M_2$ either the Higgsino state

$$\tilde{H}_{(12)} = \frac{1}{\sqrt{2}}(\tilde{H}_1^0 + \tilde{H}_2^0) \quad \mu < 0 \quad (92)$$

or the state

$$\tilde{H}_{[12]} = \frac{1}{\sqrt{2}}(\tilde{H}_1^0 - \tilde{H}_2^0) \quad \mu > 0 \quad (93)$$

is the LSP depending on the sign of μ .

In Figure 24¹⁰², regions in the M_2, μ plane with $\tan\beta = 2$ are shown in which the LSP is one of several nearly pure states, the photino, $\tilde{\gamma}$, the bino, \tilde{B} , a symmetric combination of the Higgsinos, $\tilde{H}_{(12)}$, or the Higgsino, \tilde{S} . The dashed lines show the LSP mass contours. The cross hatched regions correspond to parameters giving a chargino ($\tilde{W}^\pm, \tilde{H}^\pm$) state with mass $m_{\tilde{\chi}} \leq 45\text{GeV}$ and as such are excluded by LEP¹⁰³. This constraint has been extended by LEP1.5,^{104,105} and LEP2^{106,107} and is shown by the light shaded region and corresponds to regions where the chargino mass is $\lesssim 80$ GeV. The newer limit does not extend deep into the Higgsino region because of the degeneracy between the chargino and neutralino. The dark shaded region corresponds to an older limit on M_2 from the limit¹⁰⁸ on the gluino mass $m_{\tilde{g}} \leq 70$ GeV or $M_2 \leq 22$ GeV. Notice that the parameter space is dominated by the \tilde{B} or \tilde{H}_{12} pure states and that the photino (often quoted as the LSP) only occupies a small fraction of the parameter space, as does the Higgsino combination \tilde{S}^0 .

The relic abundance of LSP's is determined by solving the Boltzmann equation for the LSP number density in an expanding Universe. The technique⁹³ used is similar to that for computing the relic abundance of massive neutrinos⁹¹. The relic density depends on additional parameters in the MSSM. These include the sfermion masses, $m_{\tilde{f}}$, the Higgs pseudo-scalar mass, m_A , and the tri-linear masses A as well as two phases θ_μ and θ_A . For binos, as was the case for photinos¹⁰¹, it is possible to adjust the sfermion masses to obtain closure density. Adjusting the sfermion mixing parameters¹⁰⁹ or CP violating phases^{110,111} allows even greater freedom. In Figure 25¹¹², the relic abundance (Ωh^2) is shown in the $M_2 - \mu$ plane with $\tan\beta = 2$, $m_{\tilde{f}} = 200$ GeV. Clearly the MSSM offers sufficient room to solve the dark matter problem. Similar results have been found by other groups^{113,114,115}. In Figure 25, in the higgsino sector \tilde{H}_{12} marked off by the dashed line, co-annihilations^{116,114} between $\tilde{H}_{(12)}$ and the next lightest neutralino (also a Higgsino) were not included. These tend to lower significantly the relic abundance in much of this sector.

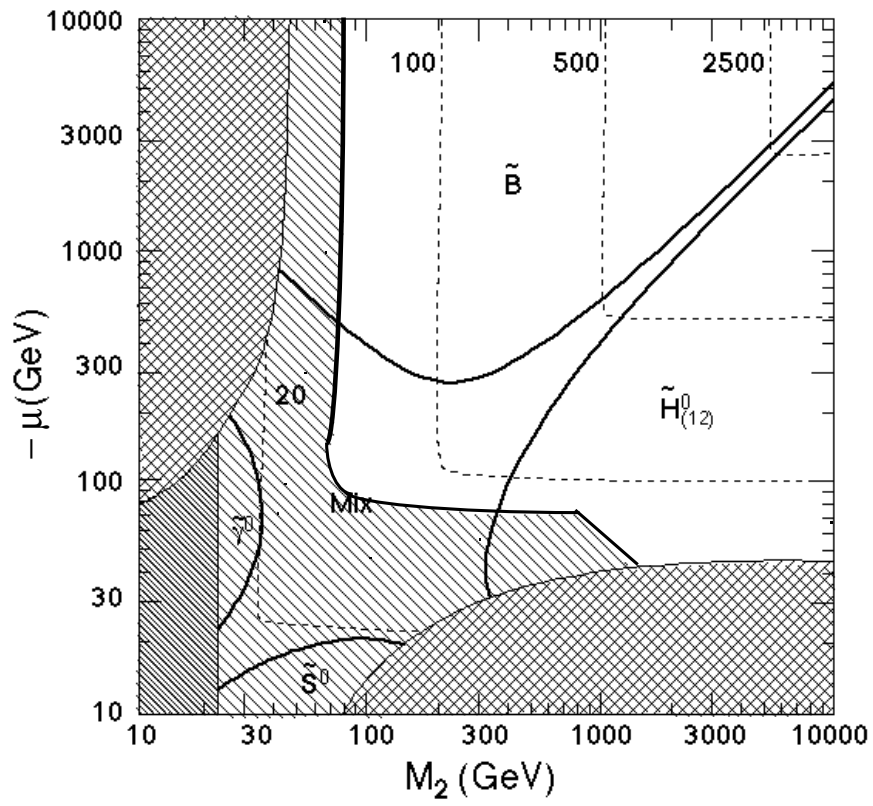


Figure 24: The M_2 - μ plane in the MSSM for $\tan \beta = 2$.

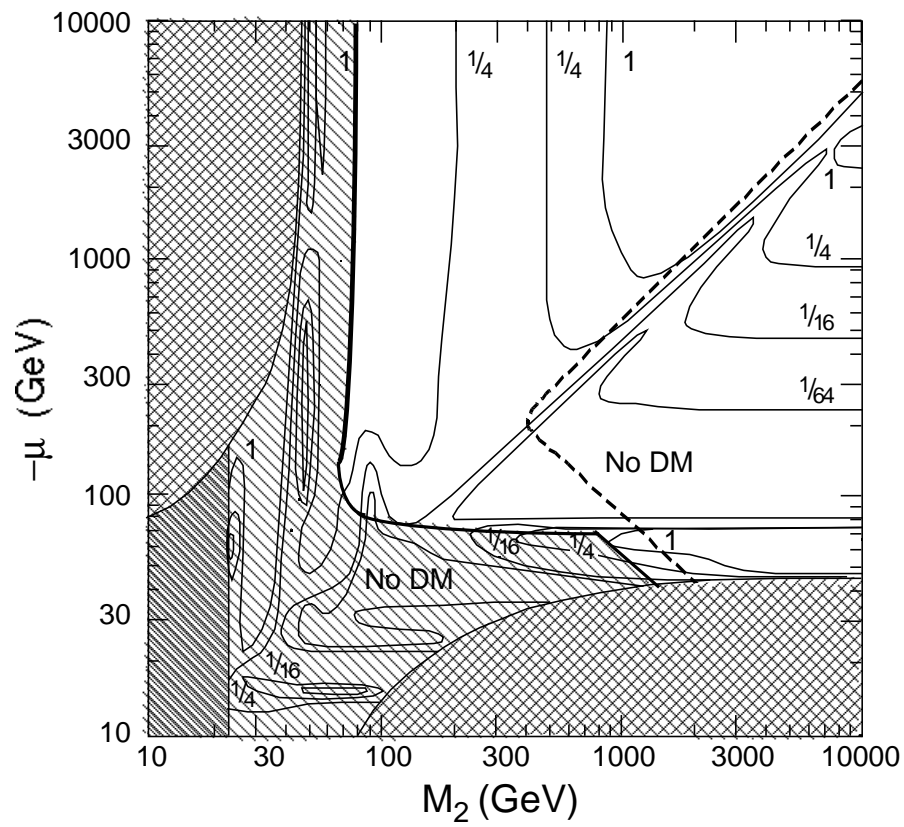


Figure 25: Relic density contours (Ωh^2) in the $M_2 - \mu$ plane.

As should be clear from figures 24 and 25, binos are a good and likely choice for dark matter in the MSSM. For fixed $m_{\tilde{f}}$, $\Omega \gtrsim 0.05$, for all $m_{\tilde{B}} = 20 - 250$ GeV largely independent of $\tan\beta$ and the sign of μ . In addition, the requirement that $m_{\tilde{f}} > m_{\tilde{B}}$ translates into an upper bound of about 250 GeV on the bino mass^{102,113}. By further adjusting the trilinear A and accounting for sfermion mixing this upper bound can be relaxed¹⁰⁹. For fixed $\Omega h^2 = 1/4$, we would require sfermion masses of order 120 – 250 GeV for binos with masses in the range 20 – 250 GeV. The Higgsino relic density on the other hand is largely independent of $m_{\tilde{f}}$. For large μ , annihilations into W and Z pairs dominate, while for lower μ , it is the annihilations into Higgs scalars which dominate. Aside from a narrow region with $m_{\tilde{H}_{12}} < m_W$ and very massive Higgsinos with $m_{\tilde{H}_{12}} < 250$ GeV, the relic density of \tilde{H}_{12} is very low. Above about 1 TeV, these Higgsinos are also excluded.

One can make a further reduction in the number of parameters by setting all of the soft scalar masses equal at the GUT scale. In particular, setting the Higgs soft masses equal to a common sfermion mass m_o and enforcing the condition of radiative electroweak symmetry breaking fixes μ and m_A ¹¹⁷. In this case, which we can refer to as the constrained MSSM (CMSSM) the LSP is almost always a bino¹¹⁸. For a given value of $\tan\beta$, the parameter space is best described in terms of the common gaugino masses $m_{1/2}$ and scalar masses m_o at the GUT scale. In Figure 26 (taken from ref. 111) this parameter space is shown for $\tan\beta = 2$. The contours labeled by a value of p represent bino purity contours. The other contours are labeled by the value of Ωh^2 . The shaded region corresponds to regions where either the LSP is not a neutralino (but rather a stau) or there is a light chargino.

The $m_{1/2} - m_o$ parameter space is further constrained by the recent runs at LEP. In Figure 27, the constraints imposed by the unsuccessful ALEPH chargino and neutralino searches¹¹⁹ (long-dashed line) at LEP 1.5 are shown. This search could not exclude regions of parameter space for small m_o , when the sneutrino mass drops below the chargino mass. However, some of this area can be further excluded¹⁰⁵ by the limits on $m_{\tilde{\nu}}$ (short-dashed line), by the LEP limits^{106,120} on slepton production (solid line), by single-photon measurements¹²¹ (grey line), and by the D0 limit on the gluino mass¹²² (dotted line). The region of the plane in which $0.1 < \Omega_\chi h^2 < 0.3$ for some experimentally-allowed value of $\mu < 0$ is light-shaded, and the region of the plane in which $0.1 < \Omega_\chi h^2 < 0.3$ for μ determined by the CMSSM constraint on the scalar masses is shown dark-shaded. The constraint derived from the

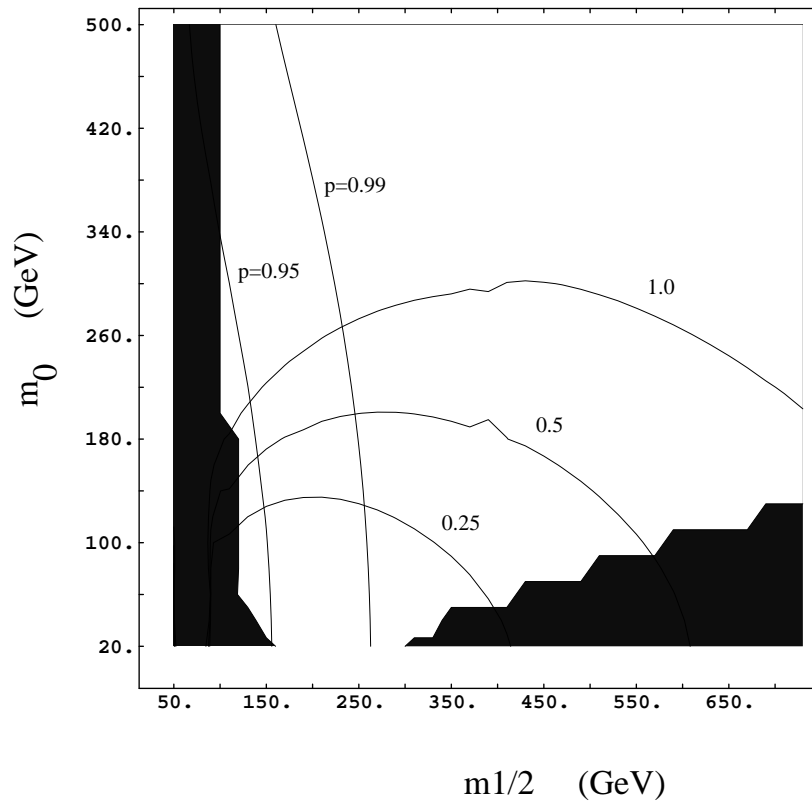


Figure 26: The $m_{1/2}$ - m_0 plane in the CMSSM for $\tan \beta = 2$.

ALEPH searches when imposing CMSSM constraints (labeled EWSB) is also shown as a solid line. The improvement in these bounds¹⁰⁷ by LEP 1.7 is illustrated in Figure 28.

The final subject that I will cover in this lecture is the question of dark matter detection and this topic will be covered in detail by J. Ellis¹²³. The best chance for the detection of baryonic dark matter, as was discussed earlier, is through gravitational microlensing^{81,83,84}. In principle, the duration of the signal should be able to determine the mass of the macho and perhaps lead to a determination of the composition of the galactic halo. The first test for the presence of neutrino dark matter is the experimental verification of neutrino masses. This will most likely be done first by observing neutrino oscillations for the case of the light neutrinos (hot dark matter). The heavy neutrinos, as explained earlier, are already excluded as dark matter experimentally.

Other non baryonic dark matter detection can be separated into two basic methods, direct and indirect. Direct detection relies on the ability to detect the elastic scattering of a dark matter candidate off a nucleus in a detector. The detection rate will depend on the density of dark matter in the solar neighborhood, $\rho \sim 0.3 \text{ GeV/cm}^3$, the velocity, $v \sim 300 \text{ km/s}$, and the elastic cross section, σ . Spin-independent interactions are the most promising for detection. Dirac neutrinos have spin-independent interactions, but as noted above, these have already been excluded as dark matter by direct detection experiments⁹⁵. In the MSSM, it is possible for the LSP to also have spin independent interactions which are mediated by Higgs exchange. These scatterings are only important when the LSP is a mixed (gaugino/Higgsino) state as in the central regions of Figures 24 and 25. Generally, these regions have low values of Ωh^2 (since the annihilation cross sections are also enhanced) and the parameter space in which the elastic cross section and relic density are large is rather limited. Furthermore, a significant detection rate in this case relies on a low mass for the Higgs scalar^{124,125}.

More typical of the SUSY parameter space is a LSP with spin dependent interactions. Elastic scatterings are primarily spin dependent whenever the LSP is mostly either gaugino or Higgsino. For Higgsino dark matter, Higgsinos with scatterings mediated by Z^0 avoid the $\tilde{H}_{(12)}$ regions of Figures 24 and 25, and as such are now largely excluded (the S^0 region does grow at low $\tan\beta$ ^{98,102}). Higgsino scatterings mediated by sfermion exchange depend on couplings proportional to the light quark masses and will have cross sections which are suppressed by $(m_p/m_W)^4$, where m_p is the proton mass. These

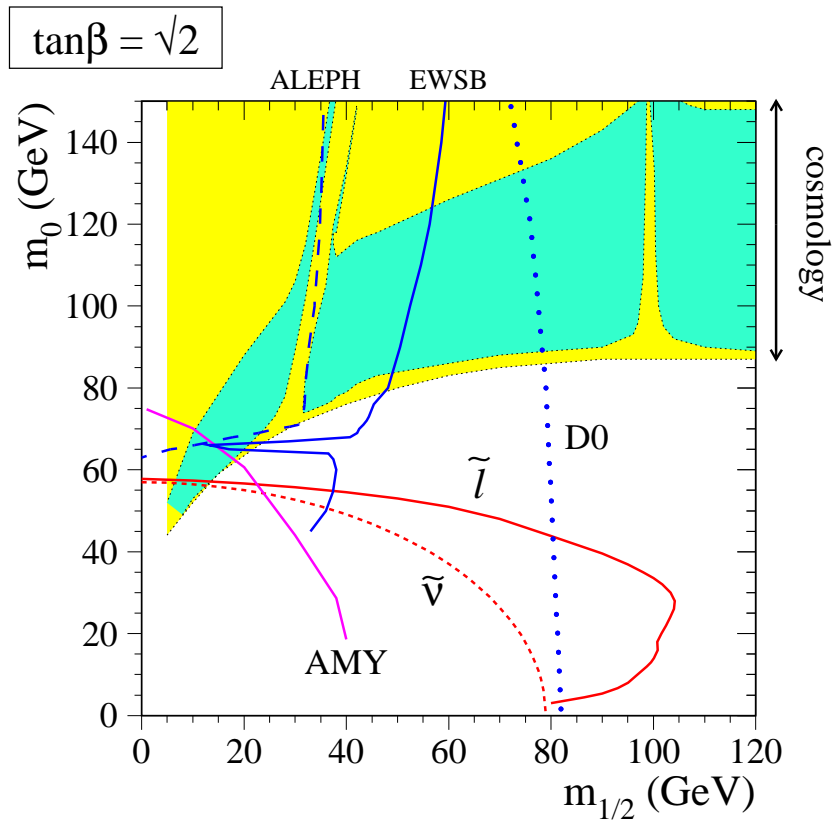


Figure 27: The $m_{1/2}$ - m_0 plane with constraints from Lep 1.5.

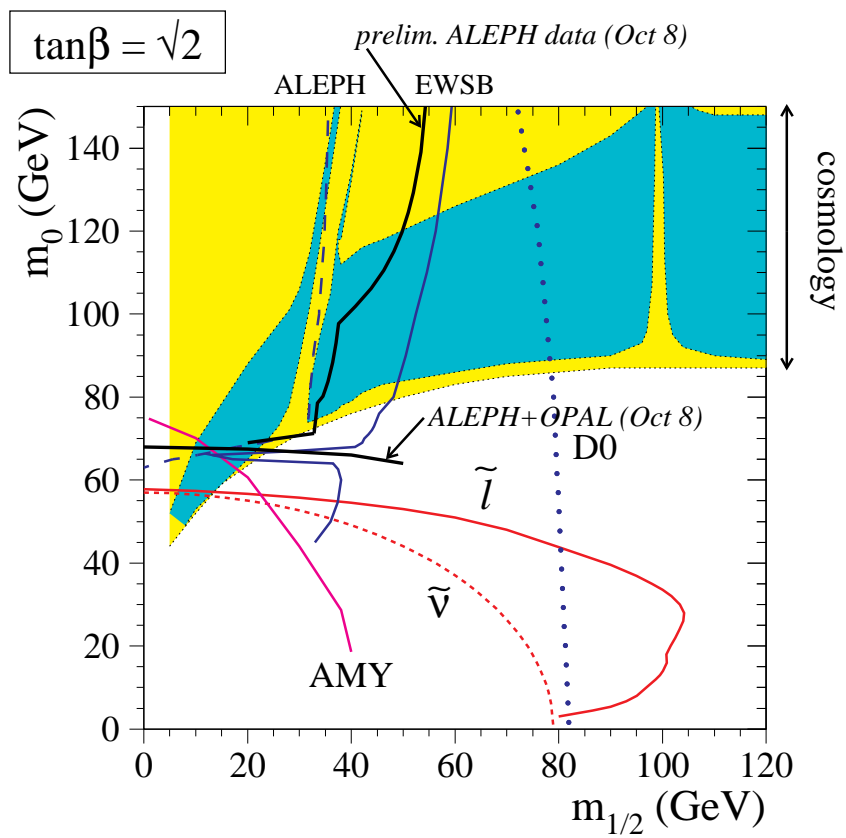


Figure 28: Same as Figure 27, but updated by the LEP 1.7 run.

rates are generally very low¹²⁵. Binos, on the other hand, will have elastic cross sections which go as $m^2/m_{\tilde{f}}^4$, where m is the reduced mass of the bino and nucleus. These rates are typically higher (reaching up to almost 0.1 events per kg-day^{125,126,127}).

Indirect methods also offer the possibility for the detection of dark matter. Three methods for indirect detection are often discussed. 1) γ -rays from dark matter annihilations in the galactic halo are a possible signature¹²⁸. In the case of the MSSM, unless the mass of the LSP is larger than m_W , the rates are probably too small to be detectable over background. 2) Dark matter will be trapped gradually in the sun, and annihilations within the sun will produce high energy neutrinos which may be detected¹²⁹; similarly, annihilations within the earth may provide a detectable neutrino signal¹³⁰. This method holds considerable promise, as there will be a number of very large neutrino detectors coming on line in the future. Finally, 3) there is the possibility that halo annihilations into positrons and antiprotons in sufficient numbers to distinguish them from cosmic-ray backgrounds¹²⁸.

Acknowledgments

This work was supported in part by DOE grant DE-FG02-94ER-40823.

References

1. see eg. J.L.Tonry, in *Relativistic Astrophysics and Particle Cosmology* ed. C.W. Akerlof and M. Srednicki (New York Academy of Sciences, New York, 1993), p.113.
2. N. Kaiser, these proceedings.
3. J.C. Mather et al., *Ap.J.* **420** (1994) 439; G. Smoot, these proceedings.
4. G. Steigman, *Ann. Rev. Astron. Astrophys.* **14** (1976) 339.
5. A.D. Sakharov, *JETP Lett.* **5** (1967) 24.
6. S. Weinberg, *Phys. Rev. Lett.* **42**, (1979) 850; D. Toussaint, S. B. Treiman, F. Wilczek, and A. Zee, *Phys. Rev.* **D19** (1979) 1036.
7. K.A. Olive, in the proceedings of the 33rd International Winter School on Nuclear and Particle Physics, "Matter Under Extreme Conditions", Feb. 27 - March 5 1994, Schladming Austria, eds. H. Latal and W. Schweiger (Springer-Verlag, Berlin, 1994) pp.1-37, hep-ph/9404352.
8. for reviews see: A.D. Linde, Particle Physics And Inflationary Cosmology

- Harwood (1990); K.A. Olive, *Phys.Rep.* **C190**(1990) 307.
9. T.P. Walker, G. Steigman, D.N. Schramm, K.A. Olive and K. Kang, *Ap.J.* **376** (1991) 51.
 10. B.D. Fields and K.A. Olive, *Phys. Lett.* **B368** (1996) 103; B.D. Fields, K. Kainulainen, D. Thomas, and K.A. Olive, astro-ph/9603009, *New Astronomy* **1** (1996) 77.
 11. G. Gamow, *Phys. Rev.* **74** (1948) 505; G. Gamow, *Nature* **162** (1948) 680 R.A. Alpher and R.C. Herman, *Nature* **162** (1948) 774.
 12. D. Thomas, D. Schramm, K.A. Olive, and B. Fields, *Ap.J.* **406** (1993) 569.
 13. Review of Particle Properties, *Phys. Rev.* **54** (1996) 1.
 14. N. Hata, R.J. Scherrer, G. Steigman, D. Thomas, and T.P. Walker, *Ap.J.* **458** (1996) 637.
 15. B.E.J. Pagel, E.A. Simonson, R.J. Terlevich and M. Edmunds, *MNRAS* **255** (1992) 325.
 16. E. Skillman and R.C. Kennicutt, *Ap.J.* **411** (1993) 655; E. Skillman, R.J. Terlevich, R.C. Kennicutt, D.R. Garnett, and E. Terlevich, *Ap.J.* **431** (1994) 172; E. Skillman et al., *Ap.J. Lett.* (in preparation) 1996.
 17. Y.I. Izotov, T.X. Thuan, and V.A. Lipovetsky, *Ap.J.* **435** (1994) 647; *Ap.J.S.* **108** (1997) 1.
 18. K.A. Olive and G. Steigman, *Ap.J. Supp.* **97** (1995) 49.
 19. K.A. Olive and S.T. Scully, *IJMPA* **11** (1995) 409.
 20. K.A. Olive, E. Skillman, and G. Steigman, *Ap.J.* **483** (1997), astro-ph/9611166.
 21. M. Spite, P. Francois, P.E. Nissen, and F. Spite, *A.A.* **307** (1996) 172; F. Spite, in the Proceedings of the IInd Rencontres du Vietnam: The Sun and Beyond, ed. J. Tran Thanh Van et al., (Editions Frontieres, Gif sur Yvett) p. 259.
 22. P. Molaro, F. Primas, and P. Bonifacio, *A.A.* **295** (1995) L47; P. Bonifacio and P. Molaro, *MNRAS* **285** (1997) 847.
 23. F. Spite, and M. Spite, *A.A.* **115** (1982) 357; M. Spite, J.P. Maillard, and F. Spite, *A.A.* **141** (1984) 56; F. Spite, and M. Spite, *A.A.* **163** (1986) 140; L.M. Hobbs, and D.K. Duncan, *Ap.J.* **317** (1987) 796; R. Rebolo, P. Molaro, J.E. and Beckman, *A.A.* **192** (1988) 192; M. Spite, F. Spite, R.C. Peterson, and F.H. Chaffee Jr., *A.A.* **172** (1987) L9; R. Rebolo, J.E. Beckman, and P. Molaro, *A.A.* **172** (1987) L17; L.M. Hobbs, and C. Pilachowski, *Ap.J.* **326** (1988) L23; L.M. Hobbs, and J.A. Thorburn,

- Ap.J.* **375** (1991) 116; J.A. Thorburn, *Ap.J.* **399** (1992) L83; C.A. Pilachowski, C. Sneden, and J. Booth, *Ap.J.* **407** (1993) 699; L. Hobbs, and J. Thorburn, *Ap.J.* **428** (1994) L25; J.A. Thorburn, and T.C. Beers, *Ap.J.* **404** (1993) L13; F. Spite, and M. Spite, *A.A.* **279** (1993) L9. J.E. Norris, S.G. Ryan, and G.S. Stringfellow, *Ap.J.* **423** (1994) 386.
24. J. Thorburn, *Ap.J.* **421** (1994) 318.
 25. C.P. Deliyannis, P. Demarque, and S.D. Kawaler, *Ap.J.Supp.* **73** (1990) 21.
 26. V.V. Smith, D.L. Lambert, and P.E. Nissen, *Ap.J.* **408** (1992) 262; L. Hobbs, and J. Thorburn, *Ap.J.* **428** (1994) L25.
 27. G. Steigman, B. Fields, K.A. Olive, D.N. Schramm, and T.P. Walker, *Ap.J.* **415** (1993) L35.
 28. T.P. Walker, G. Steigman, D.N. Schramm, K.A. Olive and B. Fields, *Ap.J.* **413** (1993) 562; K.A. Olive, and D.N. Schramm, *Nature* **360** (1993) 439.
 29. J.L. Linsky, et al., *Ap.J.* **402** (1993) 694; J.L. Linsky, et al., *Ap.J.* **451** (1995) 335.
 30. S.T. Scully, M. Cassé, K.A. Olive, D.N. Schramm, J.W. Truran, and E. Vangioni-Flam, astro-ph/0508086, *Ap.J.* **462** (1996) 960.
 31. J. Geiss, in *Origin and Evolution of the Elements*, eds. N. Prantzos, E. Vangioni-Flam, and M. Cassé (Cambridge: Cambridge University Press, 1993), p. 89.
 32. H.B. Niemann, et al. *Science* **272** (1996) 846.
 33. C. Copi, K.A. Olive, and D.N. Schramm, astro-ph/9606156 (1996).
 34. R.F. Carswell, M. Rauch, R.J. Weymann, A.J. Cooke, and J.K. Webb, *MNRAS* **268** (1994) L1; A. Songaila, L.L. Cowie, C. Hogan, and M. Rugers, *Nature* **368** (1994) 599; M. Rugers and C.J. Hogan, *Ap.J.* **459** (1996) L1.
 35. M. Rugers and C.J. Hogan, *A.J.* **111** (1996) 2135; R.F. Carswell, et al. *MNRAS* **278** (1996) 518; E.J. Wampler, et al., *A.A.* **316** (1996) 33.
 36. D. Tytler, X.-M. Fan, and S. Burles, *Nature* **381** (1996) 207; S. Burles and D. Tytler, *Ap.J.* **460** (1996) 584.
 37. A. Songaila, E.J. Wampler, and L.L. Cowie, *Nature* **385** (1997) 137.
 38. D.S. Balser, T.M. Bania, C.J. Brockway, R.T. Rood, and T.L. Wilson, *Ap.J.* **430** (1994) 667.
 39. K.A. Olive, R.T. Rood, D.N. Schramm, J.W. Truran, and E. Vangioni-Flam, *Ap.J.* **444** (1995) 680.

40. G. Gloeckler, and J. Geiss, *Nature* **381** (1996) 210.
41. R.T. Rood, T.M. Bania, and T.L. Wilson, *Nature* **355** (1992) 618; R.T. Rood, T.M. Bania, T.L. Wilson, and D.S. Balser, 1995, in *the Light Element Abundances, Proceedings of the ESO/EIPC Workshop*, ed. P. Crane, (Berlin:Springer), p. 201.
42. B.M. Tinsley, *Fund. Cosmic Phys.*, **5** (1980) 287.
43. I. Iben, and J.W. Truran, *Ap.J.* **220** (1978) 980.
44. D. Galli, F. Palla, F. Ferrini, and U. Penco, *Ap.J.* **443** (1995) 536; D. Dearborn, G. Steigman, and M. Tosi, *Ap.J.* **465** (1996) 887.
45. S. Scully, M. Cassé, K.A. Olive, and E. Vagioni-Flam, astro-ph/9607106, *Ap.J.* **476** (1997) 521.
46. C. Charbonnel, *A. A.* **282** (1994) 811; C. Charbonnel, *Ap.J.* **453** (1995) L41; C.J. Hogan, *Ap.J.* **441** (1995) L17; G.J. Wasserburg, A.I. Boothroyd, and I.-J. Sackmann, *Ap.J.* **447** (1995) L37; A. Weiss, J. Wagenhuber, and P. Denissenkov, *A.A.* **313** (1996) 581.
47. A.I. Boothroyd, A.I. and R.A. Malaney, astro-ph/9512133.
48. K.A. Olive, D.N. Schramm, S. Scully, and J.W. Truran, astro-ph/9610039, *Ap.J.* **479** (1997) 752.
49. D. Galli, L. Stanghellini, M. Tosi, and F. Palla *Ap.J.* **477** (1997) 218.
50. L.M. Krauss and P. Romanelli, *Ap.J.* **358** (1990) 47; L.M. Krauss and P.J. Kernan, *Phys. Lett.* **B347** (1995) 347; M. Smith, L. Kawano, and R.A. Malaney, *Ap.J. Supp.* **85** (1993) 219.
51. P.J. Kernan and L.M. Krauss, *Phys. Rev. Lett.* **72** (1994) 3309.
52. A. Dar, *Ap.J.* **449** (1995) 550.
53. S. Vauclair and C. Charbonnel, *A.A.* **295** (1995) 715.
54. C.Y. Cardall and G.M. Fuller, *Ap.J.* **472** (1996) 435; N. Hata, G. Steigman, S. Bludman, and P. Langacker, *Phys.Rev.* **D55** (1997) 540.
55. G. Steigman, D.N. Schramm, and J. Gunn, *Phys. Lett.* **B66** (1977) 202.
56. B.A. Campbell and K.A. Olive, *Phys. Lett.* **B345** (1995) 429.
57. J. Yang, M.S. Turner, G. Steigman, D.N. Schramm, and K.A. Olive, *Ap.J.* **281** (1984) 493.
58. K.A. Olive, D.N. Schramm, G. Steigman, M.S. Turner, and J. Yang, *Ap.J.* **246** (1981) 557.
59. K.A. Olive and D. Thomas, *Astro. Part. Phys.* in press, hep-ph/9610319.
60. G. Steigman, K.A. Olive, and D.N. Schramm, *Phys. Rev. Lett.* **43** (1979) 239; K.A. Olive, D.N. Schramm, and G. Steigman, *Nucl. Phys.*

- B180** (1981) 497.
61. E. Vangioni-Flam and M. Cassé, *Ap.J.* **441** (1995) 471.
 62. see: J.R. Primack in *Enrico Fermi. Course 92*, ed. N. Cabibbo (North Holland, Amsterdam, 1987), p. 137; V. Trimble, *Ann. Rev. Astron. Astrophys.* **25** (1987) 425; J. Primack, D. Seckel, and B. Sadulek, *Ann. Rev. Nucl. Part. Sci.* **38** (1988) 751; *Dark Matter*, ed. M. Srednicki (North-Holland, Amsterdam, 1989).
 63. S.M. Faber and J.J. Gallagher, *Ann. Rev. Astron. Astrophys.* **17** (1979) 135.
 64. A. Bosma, *Ap.J.* **86** (1981) 1825.
 65. V.C. Rubin, W.K. Ford and N. Thonnard, *Ap.J.* **238** (1980) 471; V.C. Rubin, D. Burstein, W.K. Ford and N. Thonnard, *Ap.J.* **289** (1985) 81; T.S. Van Albada and R. Sancisi, *Phil. Trans. R. Soc. Land.* **A320** (1986) 447.
 66. M. Persic and P. Salucci, *ApJ Supp* **99** (1995) 501; M. Persic, P. Salucci, and F. Stel, to be published in *Dark Matter Proc.* of the 5th Annual October Conference in Maryland (1995).
 67. R.P. Saglia et al., *Ap.J.* **403** (1993) 567; C.M. Carollo et al., *Ap.J.* **411** (1995) 25;
 68. D. Fabricant and P. Gorenstein, *Ap.J.* **267** (1983) 535; G.C. Stewart, C.R. Canizares, A.C. Fabian and P.E.J. Nilsen, *Ap.J.* **278** (1984) 53 and references therein.
 69. R. Mushotzky, in *Relativistic Astrophysics and Particle Cosmology* ed. C.W. Akerlof and M. Srednicki (New York Academy of Sciences, New York, 1993), p. 184; J.S. Mulchaey, D.S. Davis, R.F. Mushotzky, and D. Burstein, *ApJ* **404** (1993) L9; M.J. Henriksen and G.A. Mamon, *Ap.J.* **421** (1994) L63.
 70. L.P. David, C. Jones, and W. Foreman, *Ap.J.* **445** (1995) 578.
 71. P.J.E. Peebles, *The Large Scale Structure of the Universe*, (Princeton University Press, Princeton, 1980).
 72. A. Dressler, D. Lynden-Bell D. Burstein, R. Davies, S. Faber, R. Terlevich, and G. Wegner, *Ap.J.* **313** (1987) L37; A. Dekel, E. Bertschinger, A. Yahil, M.A. Strauss, M. Davis, and J.P. Huchra, *Ap.J.* **412** (1993) 1.
 73. J.A. Willick, M.A. Strauss, A. Dekel, and T. Kolatt, astro-ph/9612240.
 74. J.A. Tyson, F. Valdes, and R.A. Wenk, *Ap.J.* **349** (1990) L1.
 75. W.H. Press, *Phys. Scr.* **21** (1980) 702; V.F. Mukhanov and G.V. Chibisov, *JETP Lett.* **33** (1981) 532; S.W. Hawking, *Phys. Lett.* **115B**

- (1982) 295; A.A. Starobinsky, , *Phys. Lett.* **117B** (1982) 175; A.H. Guth and S.Y. Pi, *Phys. Rev. Lett.* **49** (1982) 1110; J.M. Bardeen, P.J. Steinhardt and M.S. Turner, *Phys. Rev.* **D28** (1983) 679.
76. E.R. Harrison, *Phys. Rev.* **D1** (1979) 2726; Ya.B. Zeldovich, *M.N.R.A.S.* **160** (1972) 1P.
 77. E.L. Wright et al. *Ap.J.* **396** (1992) L13; G. Hinshaw et al., astro-ph/9601058 (1996); G. Smoot, these proceedings .
 78. J.R. Bond and A.S. Szalay, *Ap.J.* **274** (1983) 443.
 79. J.R. Bond, G. Efstathiou and J. Silk, *Phys. Lett.* **45** (1980) 1980; Ya.B. Zeldovich and R.A.Sunyaev, *Sov. Ast. Lett.* **6** (1980) 457.
 80. Hegyi, D.J. and Olive, K.A., *Phys. Lett.* **126B** (1983) 28; *Ap. J.* **303** (1986) 56.
 81. B. Paczynski, *Ap.J.* **304** (1986) 1.
 82. C. Alcock et al., *Nature* **365** (1983) 621; E. Aubourg et al. *Nature* **365** (1983) 623.
 83. C. Alcock et al., *Phys. Rev. Lett.* **74** (1995) 2867; astro-ph/9506113 (1995); E. Aubourg et al., *A.A.* **301** (1995) 1.
 84. C. Alcock et al., astro-ph/9606165 (1996).
 85. D.N. Schramm and G. Steigman, *Ap. J.* **243** (1981) 1.
 86. P.J.E. Peebles, *Ap. J.* **258** (1982) 415; A. Melott, *M.N.R.A.S.* **202** (1983) 595; A.A. Klypin, S.F. Shandarin, *M.N.R.A.S.* **204** (1983) 891.
 87. C.S. Frenk, S.D.M. White and M.Davis, *Ap. J.* **271** (1983) 417.
 88. S.D.M. White, C.S. Frenk and M. Davis, *Ap. J.* **274** (1983) 61.
 89. J.R. Bond, J. Centrella, A.S. Szalay and J. Wilson, in *Formation and Evolution of Galaxies and Large Structures in the Universe*, ed. J. Andouze and J. Tran Thanh Van, (Dordrecht-Reidel 1983) p. 87.
 90. R. Cowsik and J. McClelland, *Phys. Rev. Lett.* **29** (1972) 669; A.S. Szalay, G. Marx, *Astron. Astrophys.* **49** (1976) 437.
 91. P. Hut, *Phys. Lett.* **69B** (1977) 85; B.W. Lee and S. Weinberg, *Phys. Rev. Lett.* **39** (1977) 165.
 92. E.W. Kolb and K.A. Olive, *Phys. Rev.* **D33** (1986) 1202; E: **34** (1986) 2531; L.M. Krauss, *Phys. Lett.* **128B** (1983) 37.
 93. R. Watkins, M. Srednicki and K.A. Olive, *Nucl. Phys.* **B310** (1988) 693.
 94. see e.g. B. Adeva, et. al., *Phys. Lett.* **B231** (1989) 509; D. Decamp, et. al., *Phys. Lett.* **B231** (1989) 519; M.Z. Akrawy, et. al., *Phys. Lett.* **B231** (1989) 530; P. Aarnio, *Phys. Lett.* **B231** (1989) 539.
 95. S. Ahlen, et. al., *Phys. Lett.* **B195** (1987) 603; D.D. Caldwell, et. al.,

- Phys. Rev. Lett.* **61** (1988) 510; M. Beck et al., *Phys. Lett.* **B336** (1994) 141.
96. P. Hut and K.A. Olive, *Phys. Lett.* **B87** (1979) 144.
97. K.A. Olive and M.S. Turner, *Phys. Rev.* **D25** (1982) 213.
98. J.Ellis, J. Hagelin, D.V. Nanopoulos, K.A.Olive and M. Srednicki, *Nucl. Phys.* **B238** (1984) 453.
99. L.E. Ibanez, *Phys. Lett.* **137B** (1984) 160; J. Hagelin, G.L. Kane, and S. Raby, *Nucl., Phys.* **B241** (1984) 638; T. Falk, K.A. Olive, and M. Srednicki, *Phys. Lett.* **B339** (1994) 248.
100. see e.g. K.A. Olive and M. Srednicki, *Phys. Lett.* **205B** (1988) 553.
101. H. Golberg, *Phys. Rev. Lett.* **50** (1983) 1419; L.M. Krauss, *Nucl. Phys.* bf B227 (1983) 556.
102. K.A. Olive and M. Srednicki, *Phys. Lett.* **B230** (1989) 78; *Nucl. Phys.* **B355** (1991) 208.
103. ALEPH collaboration, D. Decamp et al., *Phys. Rep.* **216** (1992) 253.
104. ALEPH collaboration, D. Buskulic et al., CERN-PPE/96-10 (1996).
105. J. Ellis, T. Falk, K.A. Olive, M. Schmitt, *Phys. Lett.* **B388** (1996) 97.
106. ALEPH Collaboration, D. Buskulic et al., *Phys. Lett.* **B373** (1996) 246.
107. J. Ellis, T. Falk, K.A. Olive, M. Schmitt, hep-ph/9610410, (1996).
108. J. Alitti et al., *Phys. Lett.* **B235** (1990) 363.
109. T. Falk, R. Madden, K.A. Olive, and M. Srednicki, *Phys. Lett.* **B318** (1993) 354.
110. T. Falk, K.A. Olive, and M. Srednicki, *Phys. Lett.* **B354** (1995) 99
111. T. Falk and K.A. Olive, *Phys. Lett.* **B375** (1996) 196, hep-ph/9602299.
112. J. McDonald, K. A. Olive and M. Srednicki, *Phys. Lett.* **B283** (1992) 80.
113. K. Greist, M. Kamionkowski, and M.S. Turner, *Phys. Rev.* **D41** (1990) 3565.
114. M. Drees and M.M. Nojiri, *Phys. Rev.* **D47** (1993) 376.
115. J. Lopez, D.V. Nanopoulos, and K. Yuan, *Nucl. Phys.* **B370** (1992) 445.
116. K. Greist and D. Seckel, *Phys. Rev.* **D43** (1991) 3191; S. Mizuta and M. Yamaguchi, *Phys. Lett.* **B298** (1993) 120.
117. L.E. Ibanez and G.G. Ross, *Phys. Lett.* **B110** (1982) 215; L.E. Ibanez, *Phys. Lett.* **B118** (1982) 73; J. Ellis, D.V. Nanopoulos and K. Tamvakis, *Phys. Lett.* **B121** (1983) 123; L. Alvarez-Gaumé, J. Polchinski and M.B. Wise, *Nucl. Phys.* **B221** (1983) 495; K. Inoue, A. Kakuto, H. Komatsu

- and S. Takeshita, *Prog. Th. Phys.* **68** (1982) 927.
118. J. Ellis, J. Hagelin, and D.V. Nanopoulos, *Phys. Lett.* **B159** (1985) 26; M.M. Nojiri, *Phys. Lett.* **B261** (1991) 76; J. Lopez, D.V. Nanopoulos, and K. Yuan, *Phys. Lett.* **B267** (1991) 219; and *Nucl. Phys.* **B370** (1992) 445; J. Ellis, and L. Roszkowski, *Phys. Lett.* **B283** (1992) 252; M. Drees and M.M. Nojiri, *Phys. Rev.* **D47** (1993) 376; S. Kelly, J.L. Lopez, D.V. Nanopoulos, H. Pois, and K. Yuan, *Phys. Rev.* **47** (1993) 2461; S.A. Abel, S. Sarkar, and I.B. Whittingham, *Nucl. Phys.* **B392** (1993) 83; R.G. Roberts and L. Roszkowski, *Phys. Lett.* **B309** (1993) 329; R. Arnowitt, and P. Nath, *Phys. Rev. Lett.* **70** (1993) 3696; G. Kane, C. Kolda, L. Roszkowski, J. Wells, *Phys. Rev.* **D49** (1994) 6173.
119. ALEPH Collaboration, D. Buskulic et al., CERN-PPE/96-83 (submitted to *Zeitschrift für Physik*).
120. L3 Collaboration, M. Acciarri et al., CERN preprint PPE/96-29 (1996).
121. AMY Collaboration, Y. Sugimoto et al., *Phys. Lett.* **B369** (1996) 86.
122. D0 Collaboration, S. Abachi et al., *Search for Squarks and Gluinos in $p\bar{p}$ Collisions at the D0 Detector*, contributed paper No. 434 to the Int. Europhys. Conf. on High Energy Physics, Brussels, 1995.
123. J. Ellis, these proceedings.
124. R. Barbieri, M. Frigeni, and G.F. Giudice, *Nucl. Phys.* **B313** (1989) 725.
125. R. Flores, K.A. Olive and M. Srednicki, *Phys. Lett.* **B237** (1990) 72.
126. J. Ellis and R. Flores, *Nucl. Phys.* **307** (1988) 883; *Phys. Lett.* **B263** (1991) 259.
127. L. Bergstrom and P. Gondolo, *AstroPart. Phys.* **5** (1995) 263.
128. J. Silk and M. Srednicki, *Phys. Rev. Lett.* **53** (1984) 624.
129. J. Silk, K.A. Olive, and M. Srednicki, *Phys. Rev. Lett.* **55** (1985) 257.
130. L. Krauss, M. Srednicki, and F. Wilczek, *Phys. Rev.* **D33** (1986) 2079; K. Freese, *Phys. Lett.* **B167** (1986) 295.